2022

INVESTIGATION OF NOVEL LOW TEMPERATURE ELECTROLYTES FOR LITHIUM-ION BATTERIES

Undugodage Nuwanthi Dilhari Rodrigo
University of Rhode Island, urodrigo@uri.edu

INVESTIGATION OF NOVEL LOW TEMPERATURE ELECTROLYTES FOR LITHIUM-ION BATTERIES

BY

UNDUGODAGE NUWANTHI DILHARI RODRIGO

A DISSERTATION SUBMITTED IN PARTIAL FULFILLMENT OF THE

REQUIREMENTS FOR THE DEGREE OF

DOCTOR OF PHILOSOPHY

IN

CHEMISTRY

UNIVERSITY OF RHODE ISLAND

2022

DOCTOR OF PHILOSOPHY DISSERTATION

OF

UNDUGODAGE NUWANTHI DILHARI RODRIGO

APPROVED:

Dissertation Committee:

Major Professor Brett Lucht

Dugan Hayes

David Heskett

Brenton DeBoef
DEAN OF THE GRADUATE SCHOOL

UNIVERSITY OF RHODE ISLAND

2022

ABSTRACT

Improving energy storge technology is vital to the worldwide adoption of renewable energy sources as well as the growth of electromobility. Therefore, recent research has been focused on developing rechargeable lithium-ion batteries enabling high energy and power density over a wide temperature range with improved safety. Unfortunately, the performance of lithium-ion batteries is dependent upon the operating temperatures. At subzero temperature, the performance of lithium-ion battery in carbonate-based electrolytes is decreased by increased cell resistance limiting lithium-ion transportation. Therefore, adjusting the electrolyte composition through use of novel solvents, electrolyte additives, alternative lithium salts and optimized solvent blends has been reported to improve the low temperature performance of lithium-ion batteries. This dissertation is focused on understanding the performance of lithium-ion batteries in relation to the structure and composition of surface films generated with low temperature electrolytes. Galvanostatic cycling was used to characterize the electrochemical performance of half and full cells constructed using graphite and NCM523 as anode and cathode, with X-ray Photoelectron Spectroscopy (XPS), Infra-Red spectroscopy (IR), and Scanning Electron Microscopy (SEM) to investigate the surface of the graphite anode and NCM523 cathode. In chapter 2, a novel co-solvent, isoxazole (IZ), is introduced into novel electrolyte systems composed of lithium difluoro(oxalato)borate (LiDFOB) in fluoroethylene carbonate (FEC) and LiDFOB in ethylene carbonate (EC) to improve reversible cycling at low temperature, using Li/graphite cells. Using this electrolyte systems, in combination with above mentioned analytical methods, chapter 3 attempts to elucidate the relationship between the structure and composition of the Solid Electrolyte Interphase (SEI) and cycling

performance of Li/graphite half cells. Finally, in chapter 4 investigates carboxylate esters, methyl acetate (MA) and methyl propionate (MP), as co-solvent in electrolyte systems composed of carbonate/$LiPF_6$ in $LiNi_{0.5}Co_{0.2}Mn_{0.3}O_2$ (NCM523)/graphite cells with and without electrolyte additives and the effect of surface composition and structure in electrochemical performance over a wide temperature range (-20 ˚C to 45 ˚C).

ACKNOWLEDGMENTS

I would like to thank my advisor, Professor Brett Lucht for years of mentoring, advice and guidance. I could not have asked for a better advisor and a mentor. Thank you for your immense support and countless opportunities you have given me to become a better scientist throughout my graduate career. I am truly grateful for your mentorship.

I want to acknowledge US-DOE and URI for funding my research for the past five years. None of my research work have been possible without this funding. I also want to thank all my collaborators of the DOE project, especially Dr. Xiao-Qing Yang from Brookhaven National Laboratory for giving me countless opportunities to learn so much. I would also like to thank my committee members, Professor Dugan Hayes, Professor David Heskett and my committee chair Professor Arijit Bose. Thank you all for your constant support and guidance.

I thank my loving husband, Thivanka for his constant support and encouragement over the past years. We have been through thick and thin together, and I can wait to see what adventures future hold for us.

Of course, none of accomplishments would be possible without my parents, I thank my mom and dad, and my brother for many decades of support and endless love.

Finally, I thank my lab members, in particular Chamithri, Leah, Satu, Ohbyong, Maheeka, Sunhyung, Bharathy, Jongjung, Kiran, Sumanth, Zack, Kaveendi, Mickdy, Nina and Munaiah for their stimulating discussions and being a part of my family away from home.

PREFACE

This dissertation is written in manuscript format. There are 4 chapters included in this dissertation. Chapter 1 is an introduction to lithium ion batteries. Chapter 2 was published in ACS Applied Materials & Interfaces. Chapter 3 was published in the Journal of the Electrochemical Society. Chapter 4 is written as a manuscript and is currently submitted to Journal of the Electrochemical Society.

TABLE OF CONTENTS

LIST OF FIGURES

LIST OF TABLES

CHAPTER 1

Dissertation Introduction

BACKGROUND

Over the past few decades, there has been growing concern over the increase in global temperature due to the consumption of fossil fuel. As of 2019, the largest source of greenhouse gas emissions by economic sector in the United States is from electricity and transportation, accounting for more than 50%.[1] In an effort to reduce the consumption of fossil fuels, more attention has been paid to moving towards renewable energy. In 2020, only 12% of the United States' energy consumption came from renewable energy sources, whereas 35% still came from petroleum.[2] Therefore, there has been a recent surge in development of greener energy sources and energy storage technology. To date, the lithium-ion battery is the best candidate in energy storage technology, facilitating applications ranging from small scale consumer electronics to electric vehicles and large scale grid energy storage. However, continued research and development is still needed in rechargeable battery technology to make energy storage safe and affordable for all consumers.[3–5]

WORKING CONCEPT OF LITHIUM-ION BATTERIES

There are four main components in a lithium-ion full battery, namely a negative electrode (anode), a positive electrode (cathode), the electrolyte, and separator material. Graphite is the choice of anode material in commercial lithium-ion batteries due to its stable capacity (theoretical capacity of 372 mAh/g), low cost and low working potential for reversible lithium ion intercalation /de- intercalation, close to Li^0/Li^+ (-3.04 V vs SHE).[6,7] Several different types of lithiated transition metal oxides with the common formula of LMO; where L= Lithium, and M= Nickel (Ni), Cobalt (Co), and/or Manganese (Mn), and O= Oxygen; are widely used as the cathode material.[8] These cathode materials can also

reversibly intercalate/de-intercalate lithium ions at a high working potential relative to Li^0/Li^+ and serves as the lithium ion source in the battery.[6] The two electrodes are separated by a polyethylene/polypropylene separator that does not participate in any electrochemical reactions but prevents internal short circuits within the cell. Current lithium-ion battery electrolytes primarily consist of a lithium salt (eg: lithium hexafluorophosphate ($LiPF_6$)) dissolved in a mixture of cyclic and linear carbonate solvents (eg: ethylene carbonate (EC), ethyl methyl carbonate (EMC)) which have electrochemical stability over a wide operating voltage range.[6] The electrolyte facilitates the lithium ion transfer between the graphite anode and the lithiated transition metal oxide cathode during the operation of the battery.

When charging a battery under the applied voltage, oxidation occurs at the lithiated transition metal oxide (cathode) and lithium ions are shuttled from the cathode through the electrolyte and intercalate into graphite (anode) accompanied by electrons which travel through the external circuit, causing reduction to occur at the graphite anode. The reversible process occurs during the discharge of the battery, where lithium ions de-intercalate from the anode, travel through the electrolyte, and re-intercalate into the cathode. As the discharge process is spontaneous, the electrons passing through the external circuit can be used to perform work on a load.[9] The electrochemical redox reactions occurring at each electrode during the operation are as follows:

Negative: $C + x\,Li^+ + x\,e^- \rightleftharpoons Li_xC$

Positive: $LiCoO_2 \rightleftharpoons y\,Li^+ + y\,e^- + Li_{1-y}CoO_2$

Full Cell: $LiCoO_2 + y/x\,C \rightleftharpoons y/x\,Li_xC + Li_{1-y}CoO_2$

Furthermore, during the initial formation cycles, electrolyte reacts on the surface of graphite to a form a surface film known as the Solid Electrolyte Interphase (SEI); formation of the SEI is unavoidable since the working potential of the graphite electrode lies beyond the thermodynamic stability window of typical carbonate-based LIB electrolytes.[10–12] The SEI is electronically insulating but ionically conductive meaning the SEI acts as a passivating layer to allow transfer of lithium ions and prevent further decomposition of the electrolyte.[13] The chemical composition of the SEI depends on the electrolyte formulation as it consists of organic and inorganic electrolyte decomposition products.[10] Generation of a stable SEI is important as it allows lithium ion batteries to be charged and discharged for thousands of cycles with high efficiency.

REVIEW OF THE PROBLEM

As lithium-ion batteries have become a popular choice in powering all electric and hybrid vehicles, there are still improvements needed to give a higher energy density, a stable cycle life, and increased safety before being successfully adapted into the industry. Furthermore, reduced energy and power density at subzero temperatures limits the application of lithium-ion batteries over a wide operating temperature range. Therefore, the design of new electrolyte systems composed of different solvent combinations, salts and additives not only gives desirable physical properties such as low viscosity, low melting point, high Li^+ ion conductivity, but is also able to form stable and low impedance surface films on both anode and cathode surfaces which are critical for improved performance at low temperature.[14–16] Therefore, this dissertation presents the investigation of novel low temperature electrolyte formulations for improving low temperature performance of lithium-ion batteries and understanding the role of the structure and the composition of the

surface film generated as it relates to the performance.

REFERENCES

1. United States Environmental Protection Agency, "Sources of Greenhouse Gas Emissions", https://www.epa.gov/ghgemissions/sources-greenhouse-gas-emissions (Acessed 02/14/22)

2. U.S. Energy Information Administration, "Renewable energy explained", https://www.eia.gov/energyexplained/renewable-sources/ (Acessed 02/14/22)

3. Y. Zhang, T.-T. Zuo, J. Popovic, K. Lim, Y.-X. Yin, J. Maier, and Y.-G. Guo, *Materials Today*, **33**, 56–74 (2020)

4. A. Masias, J. Marcicki, and W. A. Paxton, *ACS Energy Letters*, **6**, 621–630 (2021).

5. F. Schipper, E. M. Erickson, C. Erk, J.-Y. Shin, F. F. Chesneau, and D. Aurbach, *Journal of The Electrochemical Society*, **164**, A6220–A6228 (2017).

6. K. Xu, *Chemical Reviews*, **104**, 4303–4417 (2004).

7. R. Wagner, N. Preschitschek, S. Passerini, J. Leker, and M. Winter, *Journal of Applied Electrochemistry*, **43**, 481–496 (2013).

8. A. Manthiram, *ACS Central Science*, **3**, 1063–1069 (2017).

9. ENERGY.GOV Office of Science, DOE Expalins…Batteries " How Lithium-ion Batteries Work" https://www.energy.gov/science/doe-explainsbatteries (Accesed 02/14/22)

10. D. Aurbach et al., *Journal of The Electrochemical Society*, **142**, 2882–2890 (1995).

11. K. Xu, *Chemical Reviews*, **114**, 11503–11618 (2014).

12. L. Xing, X. Zheng, M. Schroeder, J. Alvarado, A. V. W. Cresce, K. Xu, Q. Li, and W.Li, *Accounts of Chemical Research*, **51**, 282–289 (2018).

13. S. K. Heiskanen, J. Kim, and B. L. Lucht, *Joule*, **3**, 2322–2333 (2019).

14. J. Hou, M. Yang, D. Wang, and J. Zhang, *Advanced Energy Materials*, **10**, 1–23 (2020).

15. S. S. Zhang, K. Xu, and T. R. Jow, *Electrochimica Acta*, **48**, 241–246 (2002).

16. S. S. Zhang, K. Xu, and T. R. Jow, *Journal of Power Sources*, **115**, 137–140 (2003).

CHAPTER 2

A Novel Low Temperature Electrolyte Using Isoxazole as Main Solvent for Lithium-Ion Batteries

Sha Tan[1a], U. Nuwanthi D. Rodrigo[1b], Zulipiya Shadike*[a], Brett Lucht*b, Kang Xu[c], Chunsheng Wang[d], Xiao-Qing Yang*[a], Enyuan Hu*[a]

[a] *Chemistry Division, Brookhaven National Laboratory, Upton NY 11973, USA*

[b] *Department of Chemistry, University of Rhode Island, Kingston, RI 02881, USA*

[c] *Battery Science Branch, Energy and Biomaterials Division, Sensor and Electron Devices Directorate, US Army Research Laboratory, Adelphi, MD, USA*

[d] *Department of Chemical and Biomolecular Engineering, University of Maryland, College Park, MD, USA*

S. Tan and U, N. Rodrigo contributed equally

**Corresponding authors: zshadike@bnl.gov ,blucht@uri.edu , xyang@bnl.gov, enhhu@bnl.gov*

The following manuscript was published in the ACS Applied Materials and Interfaces

ABSTRACT

A novel electrolyte system with excellent low temperature performance for lithium-ion batteries has been developed and studied. It was discovered for the first time in this work that when isoxazole (IZ) was used as main solvent, the ionic conductivity of the electrolyte for Li-ion batteries is more than doubled in a temperature range between -20 ^{o}C to 20 ^{o}C compared to the baseline electrolyte using ethylene carbonate-ethyl methyl carbonate (EC-EMC) as solvents. To solve the problem of the solvent co-intercalation into the graphite anode and/or electrolyte decomposition, lithium difluoro(oxalato)borate (LiDFOB) salt and fluoroethylene carbonate (FEC) additive were used to form stable solid electrolyte interphase (SEI) on the surface of graphite anode. Benefitted from the high ionic conductivity at low temperature, cells using new electrolyte with 1M LiDFOB in FEC:IZ (1:10, vol%) solvents demonstrated very high 187.5 mAh g^{-1} reversable capacity at -20 ^{o}C while the baseline electrolyte only delivered 23.1 mAh g^{-1} reversable capacity.

INTRODUCTION

As the state-of-art energy storage technology, lithium ion battery (LIB) consisting of graphite anode, lithium metal oxide cathode, and carbonate electrolyte, has been widely used as power source for various consumer electronic devices, as well as for electric vehicles1-5.However, when operated at low temperatures (below 0°C) the power density and energy density of LIB are seriously reduced. For example, the energy density and power density of LIB at -40°C can only retain 5% and 1.25% of their value at room temperature respectively.6 More serious problem is the lithium plating on graphite during low temperature charging due to the significantly increased polarization for LIB operated at subzero environments. This low temperature operation limitation greatly hindered LIB applications in outer space systems and electric vehicles. It has been reported that such poor electrochemical performance of LIB can be mainly attributed to the sluggish kinetics at low temperature, due to decreased electrolyte ionic conductivity and increased electrolyte/electrode interphase impedance. Therefore, developing new electrolyte systems with high ionic conductivity and low interface impedance at low temperature is critically needed. Currently, the electrolytes used in commercial LIBs are formulated with cyclic ethylene carbonate (EC) and various linear carbonates, in which EC is a critical solvent due to its capability to form stable solid electrolyte interphase (SEI) in protecting graphite anode from co-intercalation of solvent during charge-discharge cycling. Unfortunately, the high melting point of EC (36.4 °C) greatly limits ionic transportation at subzero environments. Aimed to enhance ionic conductivity, low melting point and low viscosity solvents/co-solvents have been extensively introduced and studied for low temperature electrolytes. For example, Smart et al. introduced various carboxylate esters (such as ethyl acetate (EA), methyl acetate (MA), isopropyl acetate (IPA), ethyl propionate (EP), etc.)

into electrolyte and demonstrated greatly improved discharge capacity at -20°C.7-9 In addition, some nitriles and fluorinated solvents have also been utilized as low viscosity/low melting point electrolyte solvents and showed improved performance.10, 11 Low temperature not only significantly reduces ionic conductivity in bulk electrolyte, but also increase the impedance at the interphases.12 The strategy of adding good SEI formation additives such as lithium difluorophosphate, lithium difluorobis(oxalato) phosphate, dimethyl sulfide, etc. have been extensively studied .13-18

Apart from optimizing electrolyte formulations and introducing various additives, another approach is searching for new electrolyte solvents. Carbonates including cyclic carbonates and linear carbonates are widely used in commercial electrolyte systems today for LIBs together with additives that can form stable SEI. Other solvents such as nitriles have also been utilized as electrolyte solvents. However, only limited number of reports on the new solvent studies for low temperature electrolytes10, 19, 20 have been published, regardless of searching new electrolyte solvents with low melting point and low viscosity is a quite important strategy for low temperature electrolyte development.

In this work, we have discovered a new electrolyte solvent, isoxazole (IZ), that has high potential to improve low temperature performance of LIBs. IZ is a five-membered aromatic heterocyclic compound with two electronegative heteroatoms, nitrogen and oxygen (Figure 2-1a). This compound has been used as an important component for various synthetic procedures and pharmacological chemistries.21, 22 Although IZ has been extensively applied in synthetic and pharmacological fields, the reports about its electrolyte applications are quite limited. There is one patent in the literature about using IZ as electrolyte additive to prevent self-discharge,19 but no report on using it as electrolyte

solvent has been found. The most attractive properties of IZ are its high boiling point (~95 °C) and low melting point (~-67 °C) which ensure a wide temperature range in liquid phase. Furthermore, the high dipole moment and low viscosity of isoxazole ensures facile Li ion transportation even at low temperatures.23 We prepared a series of IZ-based electrolytes with various salts and additives and studied their electrochemical performance at different temperatures. It was found that the ionic conductivity of IZ-based electrolyte (1M LiPF6 in EC/IZ v: 1/10) is almost 3 times higher than the baseline electrolyte (1M LiPF6 in EC/EMC wt: 3/7) at both room temperature and -20 °C. This result is very impressive and encouraging. Unfortunately, the 1M LiPF6 in EC/IZ (1/10) electrolyte was not able to form stable SEI to prevent the co-intercalation of solvent molecule into graphite anode. Therefore, different electrolyte formulations using different salts and additives were studied to solve this problem. We discovered that IZ-based electrolyte using lithium difluoro(oxalato)borate (LiDFOB) salt and fluoroethylene carbonate (FEC) additive achieved the best Li/graphite long term cycling performance. Furthermore, the ionic conductivity of this IZ-based electrolyte is 2 times higher than the baseline electrolyte in temperature range between 20 °C and -20 °C, demonstrating surprisingly high ionic conductivity compared to baseline electrolytes. This IZ-based electrolyte delivered 9 times higher charge/discharge capacities at -20°C than the baseline electrolyte.

EXPERIMENTAL

As shown below, isoxazole (IZ)-based electrolytes were prepared inside of Ar-filled glove box following the compositions below:

Electrolyte Compositions
1M $LiPF_6$ in EC/EMC (3/7, wt%)
1M $LiPF_6$ in IZ/EC (10/1, vol%)
1M LiDFOB in IZ/EC (10/1, vol%)
1M LiFSI in IZ/EC (10/1, vol%)
1M LiTFSI in IZ/EC (10/1, vol%)
1M LiDFOB in IZ
1M LiDFOB in IZ/EC (7/3, vol%)
1M LiDFOB in IZ/FEC (10/1, vol%)
1M LiDFOB + LiFSI (molar ratio: 1/1) in IZ/EC (10/1, vol%)

Graphite slurry was prepared by mixing active material (graphite powder, 80 wt%), conducting agent (super P carbon, 10 wt%), and binder (PVDF, 10 wt%), then dispersing the mixture in N-methyl-2-pyrrolidone (NMP). The slurry was then uniformly coated onto Cu foil and vacuum dried at 80 °C overnight. The dried graphite electrodes were punched into ½ inch diameter discs with an active material mass loading of 3~4 mg.

The galvanostatic charge/discharge curves of Li/graphite cells were tested using the Neware battery cycler. For these experiments, the 2032-type coin cells were assembled inside Ar-filled glove box with polypropylene separator (Celgard 3501). The Li/graphite half-cell was cycled in the voltage range of 0.01~2.00 V with a current density of C/10 which was calculated based on the theoretical capacity of 370 mAh g^{-1} for graphite anode. For the low temperature electrochemical performance, Li/graphite cells were activated at room temperature at C/10 for two cycles to stabilize interphases. Afterwards, charge/discharge performance at different temperatures between -30 ℃ and 20 ℃ were tested using MTI battery cycler and Tenney environment chamber.

Electrochemical impedance spectroscopy (EIS) was used to calculate ionic conductivity

using symmetric cells with two platinum electrodes symmetrically placed in the electrolyte solution. After collecting EIS spectra via impedance analyzer (BioLogic SAS) at open circuit voltage within 1HZ~100kHz at controlled temperatures using Tenney test chamber, solution resistance at various temperatures was obtained, and it can be converted to ionic conductivity following the equation:[24]

$$R = \rho \frac{l}{A}$$

Where l is the distance between the electrodes, A is the Pt electrode area, R represents solution resistance and ρ is the resistivity. The reciprocal of resistivity is the ionic conductivity. To obtain the l and A, standard solution KCl was used.

Coin cells (CR2032) were assembled in an Ar filled glovebox. A single-side coated graphite anode (94.5% active material, 8 mg/cm^2 active material loading, 5.5% conductive carbon, carboxymethyl cellulose (CMC) + styrene butadiene rubber (SBR) binder), a Li metal foil disk (16 mm in diameter) as the counter electrode, a Celgard 2325 separator and 100 µl of electrolyte were used in the coin cell. For the XPS analysis, constructed cells were cycled at room temperature within a voltage range of 0.01- 2.00 V with a current corresponding to C/10 for five formation cycles using an Arbin LBT21084 high precision battery cycler. After completing the formation cycles, cells were dissembled in an Ar-filled glove box. Delithiated graphite electrodes extracted from the cells were rinsed with 3×500µl extra dry dimethyl carbonate (DMC, 99+%, Acros) to remove the residual electrolyte and dried under vacuum overnight. X-ray photoelectron spectroscopy (XPS) measurements were carried out using a Thermo K-alpha system using Al Kα radiation (hυ=1486.6 eV) under ultra-high vacuum conditions (<1×10^{-12} atm) with a measured spot size of 400 µm. Samples were transferred into the XPS chamber with a vacuum transfer vessel to avoid

exposure to air. The binding energy was corrected based on the C 1s of C-C at 285.0 eV. The spectra obtained were analyzed using Thermo Advantage software (version 5.984).

RESULTS AND DISCUSSION

To quickly evaluate the potential of using IZ-based electrolytes for low temperature application, the ionic conductivity of IZ-based electrolyte (1M $LiPF_6$ in EC/IZ v: 1/10) in comparison with baseline electrolyte (1M $LiPF_6$ in EC/EMC wt: 3/7) at both room temperature and -20 °C were carried out using electrochemical impedance spectroscopy and the results are shown in Figure 2-1b. It can be seen that the ionic conductivity of IZ-based electrolyte reached 27.5 mS cm^{-1} at room temperature and retained as high as 15 mS cm^{-1} at -20 °C, both values are more than 3 times higher than those for the baseline electrolytes (10 mS cm^{-1} at room temperature and 3 mS cm^{-1} at -20 °C).

Although 1M $LiPF_6$ in EC/IZ (1/10, vol%) electrolyte demonstrated surprisingly high ionic conductivity, it couldn't support stable Li/graphite charge/discharge as shown in the green curves in Figure 2-2a. It's well accepted that lithium salt is an essential part of battery electrolyte, which could affect the ionic conductivity, transference number, and the SEI formation.[25] Therefore, to explore the proper salt for IZ solvent, electrochemical performances of cells using different salts in IZ solvent has been studied. The first charge/discharge curves of Li/graphite cells with different electrolytes at room temperature are shown in Figure 2-2a. It can be clearly seen that cells using LiFSI, $LiPF_6$ and LiTFSI salts all show a long plateau around 1.0V during discharging, which is a typical behavior of solvent co-intercalation and/or decomposition, because of no stable SEI was formed. As a result, cells can't be charged reversibly. Therefore, a good SEI forming salt was used. After replacing salt by LiDFOB, a plateau corresponding to LiDFOB reduction at ~1.7 V

appeared, the co-intercalation of solvent at ~1.0V was significantly suppressed and Li/graphite cell was successfully charged back. These phenomena indicated that IZ decomposition products alone could not form stable SEI to protect graphite from solvent co-intercalation and decomposition. With the assistance of the better SEI forming salt, LiDFOB, a stable SEI was able to be formed on graphite anode and the co-intercalation was suppressed.

By using the LiDFOB salt in IZ-based electrolyte, the solvent co-intercalation was partially suppressed. However, the electrochemical performance was still far from satisfactory, as shown by the poor Coulombic efficiency (56.5%) for the first cycle. It's well-accepted that EC can participate in the SEI formation and passivate the graphite electrode very well. Therefore, EC has been widely used in electrolyte to improve SEI properties.[26] Figure 2-2b-d show the Li/graphite cell performance using IZ-based electrolytes with different amount of EC. Without the addition of EC (Figure 2-2b), large irreversible capacity (CE: 43.5%) of the first cycle was observed， indicating some degree of solvent co-intercalation. When 10% EC was added to the electrolyte, the electrochemical performance was significantly improved and the irreversible capacity generated between 1.0~0.2V was decreased, indicating the suppression of solvent co-intercalation. However, when larger amount of EC (3:7 ratio of EC:IZ) was used, the electrochemical performance shown in Fig. 2-2d is worse than that for EC/IZ (1/10) shown in Figure 2-2c. This might be caused by the severe irreversible co-intercalation in the higher EC content electrolyte, resulting in low capacity for the several initial cycles and very low Coulombic efficiency (36.3%) for the first cycle.

The electrochemical performance for longer term cycling of Li/graphite cell using IZ/EC

(10/1) at room temperature is shown in Figure 2-3a. After 200 cycles, there was only a small percentage of capacity loss (5.97%) was observed. The fluorinated ethylene carbonate, FEC was also widely used in electrolytes due to its outstanding ability to form stable SEI on graphite anode. After replacing EC by FEC, the electrochemical performance was significantly improved as shown in Figure 2-3b. It can be clearly seen that higher first cycle CE (57.5%) was obtained, and the cycling stability of Li/graphite cell was significantly improved. The cyclic performance of Li/graphite cells cycled in IZ/EC and IZ/FEC based electrolytes are shown in Figure 2-3c. No obvious capacity decay over 200 cycles with capacity retention of 99.33% can be seen for the cell cycled in IZ/FEC based electrolyte. In comparison, the reversible capacity of the cell cycled in IZ/EC based electrolyte gradually decreased after 150 cycles and a capacity retention of 94.03% was obtained after 200 cycles. These results demonstrated that the combination of LiDFOB and FEC is capable to form stable SEI on graphite anode and enable better long term cyclic performance. Therefore, the electrolyte containing 1M LiDFOB in IZ/FEC was further used for the low temperature performance studies.

To apply the IZ-based electrolytes for low temperature application, the ionic conductivity at different temperatures was investigated using electrochemical impedance spectroscopy. As shown in Figure 2-4a, baseline electrolyte resistance increased rapidly with decreasing temperature, which hindered ionic transportation considerably at low-temperature conditions. In contrast, IZ/FEC based electrolyte demonstrated only slightly increased resistance as shown in Figure 2-4b. The calculated ionic conductivity based on the EIS results is shown in Figure 2-4c. Because the solubility of LiDFOB in IZ is lower than $LiPF_6$ and the viscosity of FEC is higher than EC, the ionic conductivity of 1M LiDFOB in

IZ/FEC is lower than that of 1M $LiPF_6$ in IZ/EC shown in Figure 2-1b. Among all the measured temperatures, the IZ/FEC based electrolyte exhibited higher ionic conductivity than the baseline electrolyte. Particularly, an ionic conductivity of ~10 mS cm^{-1} was achieved at -20°C, which is two times higher than that of baseline electrolytes and thus rendering a promising performance at low temperature. The charge/discharge performances of cells using baseline and IZ/FEC based electrolytes were also investigated at different low temperatures of 0 ℃, -10℃, -20℃ and -30℃. It can be clearly seen from Figure 2-4d and 2-4e, higher charge/discharge capacities were obtained with IZ electrolyte at various temperatures. It is interesting to point out that the cell cycled in baseline electrolyte only delivered a reversible capacity of 23.1 mAh g^{-1} at -20°C. In contrast, the cell using IZ/FEC based electrolyte delivered high reversible capacity of 187.5 mAh g^{-1} with a high coulombic efficiency of 99.7%. Even at -30 ℃, the cell using IZ/FEC based electrolyte could still deliver a high reversible capacity of 120 mAh g^{-1} with small overpotential than the cell using baseline electrolyte. In comparison, the reversible capacity of the cell using baseline electrolyte was as low as 10 mAh g^{-1}. In addition, such excellent low temperature performance of IZ electrolyte was further demonstrated through stable cyclic performance at 0°C shown in Figure 2-4f. It can be seen that after 10 charge/discharge cycles, the cell with IZ electrolyte still delivered a reversible capacity of 322 mAh g^{-1}, while only a reversible capacity of 250 mAh g^{-1} can be achieved for the cell with baseline electrolyte. Furthermore, unlike IZ electrolyte which already delivers a stable capacity in the second cycle, the baseline electrolyte needs several cycles to deliver a stable capacity as shown in Figure 2-4f. This is likely due to the unstable interphase in baseline electrolyte at low temperature. These results provide further evidence showing that IZ is a

promising electrolyte solvent for low temperature application.

In order to better understand the origin of improved cycling performance, the surface films formed on the graphite electrodes were investigated using XPS. The C1s, O1s, F1s, B1s and N1s spectra of the pristine graphite and electrodes cycled using baseline and 1M LiDFOB in IZ/FEC (10/1, vol%) electrolytes are plotted in Figure 2-5. The C1s spectrum of pristine electrode contains 3 peaks. The peak at 285 eV is attributed to C-C in graphite, while peaks at 286.3 eV and 287.6 eV are characteristics of the CMC/SBR binder.[27] After the formation cycle in baseline and IZ electrolytes, graphite signal weakened and binder signal disappeared as shown in Figure 2-5a due to SEI formation on the anode surface. The anodes cycled in baseline electrolyte contains a C1s peak at 290 eV, consistent with generation of lithium alkyl carbonates and lithium carbonate, which are reported in the literature as the primary decomposition products of carbonate solvents reduction for SEI formation.[25, 26, 28] The C1s, O1s, F1s, B1s and N1s spectra for the electrodes cycled with1M LiDFOB in IZ/FEC are dominated by decomposition products of LiDFOB. In C1s spectra, peaks are observed at 289.1 eV (C=O) and 286.7 eV (C-O) consistent with formation of oxalate species from LiDFOB decomposition.[29, 30] The importance of LiDFOB reduction in SEI generation is further evidenced by a broad peak at 193 eV (B-F) in B1s spectra.[25, 30] The presence of N-O and N-C peaks in N1s spectrum in IZ-based electrolyte is an evidence of the reduction of nitrogen-containing isoxazole in generating the SEI during the formation cycle. For all the electrolytes tested, the O1s spectra contain a broad peak centered around 533 eV, characteristic of a mixture of C-O and C=O containing species and is consistent with the C1s spectra. Because of the dominance of LiDFOB reduction, C=O peak with much higher intensity was observed in IZ/FEC electrolyte O 1s spectrum.

Major differences between the SEI composition formed in baseline and IZ/FEC electrolytes are observed in F1s spectra. Two peaks corresponding to LiF (685 eV) and $Li_xPF_yO_z$ (687.8 eV) are observed for the baseline electrolyte originated from $LiPF_6$ decomposition. As for IZ/FEC electrolyte, besides the peak representing LiF generated from FEC and LiDFOB reduction, there is an additional peak at 687 eV which is assigned to B-F containing species of the cross-linked boron-containing polymers in the SEI resulted from the LiDFOB decomposition.[25, 31] Overall, the formation of an oxalates rich SEI in IZ-based electrolytes might be the main contributor to the enhanced SEI stability and improved cycling performance.

CONCLUSIONS

IZ, a novel electrolyte solvent for low temperature LIBs, was discovered and studied. By studying salt impacts towards the electrochemical performance, LiDFOB was identified as s good salt to form stable SEI to protect graphite anode and enable Li/graphite cell cycling. After coupling with 10% FEC additive, the electrochemical performance was further improved. Compared with baseline electrolyte, isoxazole electrolyte has very high ionic conductivity at both room and low temperatures, thereby is able to deliver reversible capacities of 187.5 mAh g^{-1} at -20°C, which is about 9 times higher than those delivered by baseline electrolyte.

ACKNOWLEDGMENTS

This work was supported by the Assistant Secretary for Energy Efficiency and Renewable Energy, Vehicle Technology Office of the U.S. DOE through Applied Battery Research for Transportation (ABRT) program under contract No. DE-SC0012704. The electrodes used in this study were produced at the U.S. Department of Energy's (DOE) CAMP (Cell Analysis, Modeling and Prototyping) Facility, Argonne National Laboratory. The CAMP Facility is fully supported by the DOE Vehicle Technologies Office (VTO).

REFERENCES

1. Armand, M.; Tarascon, J. M., Building better batteries. *Nature* **2008,** *451* (7179), 652-657.

2. Tarascon, J. M.; Armand, M., Issues and challenges facing rechargeable lithium batteries. In *Materials for Sustainable Energy*, Co-Published with Macmillan Publishers Ltd, UK: 2010; pp 171-179.

3. Barré, A.; Deguilhem, B.; Grolleau, S.; Gérard, M.; Suard, F.; Riu, D., A review on lithium-ion battery ageing mechanisms and estimations for automotive applications. *Journal of Power Sources* **2013,** *241*, 680-689.

4. Wang, Y.; Liu, B.; Li, Q.; Cartmell, S.; Ferrara, S.; Deng, Z. D.; Xiao, J., Lithium and lithium ion batteries for applications in microelectronic devices: A review. *Journal of Power Sources* **2015,** *286*, 330-345.

5. Choi, S.; Wang, G., Advanced Lithium-Ion Batteries for Practical Applications: Technology, Development, and Future Perspectives. *Advanced Materials Technologies* **2018,** *3* (9), 1700376.

6. Nagasubramanian, G., Electrical characteristics of 18650 Li-ion cells at low temperatures. *Journal of Applied Electrochemistry* **2001,** *31* (1), 99-104.

7. Sazhin, S. V.; Khimchenko, M. Y.; Tritenichenko, Y. N.; Lim, H. S., Performance of Li-ion cells with new electrolytes conceived for low-temperature applications. *Journal of Power Sources* **2000,** *87* (1), 112-117.

8. Smart, M. C.; Ratnakumar, B. V.; Surampudi, S., Use of Organic Esters as Cosolvents in Electrolytes for Lithium-Ion Batteries with Improved Low Temperature Performance. *Journal of The Electrochemical Society* **2002,** *149* (4), A361-A370.

9. Smart, M. C.; Ratnakumar, B. V.; Chin, K. B.; Whitcanack, L. D., Lithium-Ion

Electrolytes Containing Ester Cosolvents for Improved Low Temperature Performance. *Journal of The Electrochemical Society* **2010,** *157* (12), A1361-A1374.

10. Cho, Y.-G.; Kim, Y.-S.; Sung, D.-G.; Seo, M.-S.; Song, H.-K., Nitrile-assistant eutectic electrolytes for cryogenic operation of lithium ion batteries at fast charges and discharges. *Energy & Environmental Science* **2014,** *7* (5), 1737-1743.

11. Smart, M. C.; Ratnakumar, B. V.; Ryan-Mowrey, V. S.; Surampudi, S.; Prakash, G. K. S.; Hu, J.; Cheung, I., Improved performance of lithium-ion cells with the use of fluorinated carbonate-based electrolytes. *Journal of Power Sources* **2003,** *119-121*, 359-367.

12. Zhu, G.; Wen, K.; Lv, W.; Zhou, X.; Liang, Y.; Yang, F.; Chen, Z.; Zou, M.; Li, J.; Zhang, Y.; He, W., Materials insights into low-temperature performances of lithium-ion batteries. *Journal of Power Sources* **2015,** *300*, 29-40.

13. Yang, B.; Zhang, H.; Yu, L.; Fan, W.; Huang, D., Lithium difluorophosphate as an additive to improve the low temperature performance of LiNi0.5Co0.2Mn0.3O2/graphite cells. *Electrochimica Acta* **2016,** *221*, 107-114.

14. Liao, B.; Li, H.; Xu, M.; Xing, L.; Liao, Y.; Ren, X.; Fan, W.; Yu, L.; Xu, K.; Li, W., Designing Low Impedance Interface Films Simultaneously on Anode and Cathode for High Energy Batteries. *Advanced Energy Materials* **2018,** *8* (22), 1800802.

15. Li, Q.; Lu, D.; Zheng, J.; Jiao, S.; Luo, L.; Wang, C.-M.; Xu, K.; Zhang, J.-G.; Xu, W., Li+-Desolvation Dictating Lithium-Ion Battery's Low-Temperature Performances. *ACS Applied Materials & Interfaces* **2017,** *9* (49), 42761-42768.

16. Guo, R.; Che, Y.; Lan, G.; Lan, J.; Li, J.; Xing, L.; Xu, K.; Fan, W.; Yu, L.; Li, W., Tailoring Low-Temperature Performance of a Lithium-Ion Battery via Rational

Designing Interphase on an Anode. *ACS Applied Materials & Interfaces* **2019,** *11* (41), 38285-38293.

17. Yang, T.; Fan, W.; Wang, C.; Lei, Q.; Ma, Z.; Yu, L.; Zuo, X.; Nan, J., 2,3,4,5,6-Pentafluorophenyl Methanesulfonate as a Versatile Electrolyte Additive Matches LiNi0.5Co0.2Mn0.3O2/Graphite Batteries Working in a Wide-Temperature Range. *ACS Applied Materials & Interfaces* **2018,** *10* (37), 31735-31744.

18. Liu, B.; Li, Q.; Engelhard, M. H.; He, Y.; Zhang, X.; Mei, D.; Wang, C.; Zhang, J.-G.; Xu, W., Constructing Robust Electrode/Electrolyte Interphases to Enable Wide Temperature Applications of Lithium-Ion Batteries. *ACS Applied Materials & Interfaces* **2019,** *11* (24), 21496-21505.

19. Alvarado, J.; Schroeder, M. A.; Zhang, M.; Borodin, O.; Gobrogge, E.; Olguin, M.; Ding, M. S.; Gobet, M.; Greenbaum, S.; Meng, Y. S.; Xu, K., A carbonate-free, sulfone-based electrolyte for high-voltage Li-ion batteries. *Materials Today* **2018,** *21* (4), 341-353.

20. Xu, K., Electrolytes and Interphases in Li-Ion Batteries and Beyond. *Chemical Reviews* **2014,** *114* (23), 11503-11618.

21. Ji Ram, V.; Sethi, A.; Nath, M.; Pratap, R., Chapter 5 - Five-Membered Heterocycles. In *The Chemistry of Heterocycles*, Ji Ram, V.; Sethi, A.; Nath, M.; Pratap, R., Eds. Elsevier: 2019; pp 149-478.

22. Zhu, J.; Mo, J.; Lin, H.-z.; Chen, Y.; Sun, H.-p., The recent progress of isoxazole in medicinal chemistry. *Bioorganic & Medicinal Chemistry* **2018,** *26* (12), 3065-3075.

23. Li, Z.; Carmichael, I.; Ptasinska, S., Dissociative electron attachment induced ring opening in five-membered heterocyclic compounds. *Phys Chem Chem Phys* **2018,** *20* (27), 18271-18278.

24. Hagos, T. T.; Thirumalraj, B.; Huang, C.-J.; Abrha, L. H.; Hagos, T. M.; Berhe, G. B.; Bezabh, H. K.; Cherng, J.; Chiu, S.-F.; Su, W.-N.; Hwang, B.-J., Locally Concentrated LiPF6 in a Carbonate-Based Electrolyte with Fluoroethylene Carbonate as a Diluent for Anode-Free Lithium Metal Batteries. *ACS Applied Materials & Interfaces* **2019,** *11* (10), 9955-9963.

25. Nie, M.; Lucht, B. L., Role of Lithium Salt on Solid Electrolyte Interface (SEI) Formation and Structure in Lithium Ion Batteries. *Journal of The Electrochemical Society* **2014,** *161* (6), A1001-A1006.

26. Heiskanen, S. K.; Kim, J.; Lucht, B. L., Generation and Evolution of the Solid Electrolyte Interphase of Lithium-Ion Batteries. *Joule* **2019,** *3* (10), 2322-2333.

27. El Ouatani, L.; Dedryvère, R.; Ledeuil, J. B.; Siret, C.; Biensan, P.; Desbrières, J.; Gonbeau, D., Surface film formation on a carbonaceous electrode: Influence of the binder chemistry. *Journal of Power Sources* **2009,** *189* (1), 72-80.

28. Nie, M.; Chalasani, D.; Abraham, D. P.; Chen, Y.; Bose, A.; Lucht, B. L., Lithium Ion Battery Graphite Solid Electrolyte Interphase Revealed by Microscopy and Spectroscopy. *The Journal of Physical Chemistry C* **2013,** *117* (3), 1257-1267.

29. Parimalam, B. S.; Lucht, B. L., Reduction Reactions of Electrolyte Salts for Lithium Ion Batteries: LiPF6, LiBF4, LiDFOB, LiBOB, and LiTFSI. *Journal of The Electrochemical Society* **2018,** *165* (2), A251-A255.

30. Xu, M.; Zhou, L.; Hao, L.; Xing, L.; Li, W.; Lucht, B. L., Investigation and application of lithium difluoro(oxalate)borate (LiDFOB) as additive to improve the thermal stability of electrolyte for lithium-ion batteries. *Journal of Power Sources* **2011,** *196* (16), 6794-6801.

31. Verma, P.; Maire, P.; Novák, P., A review of the features and analyses of the solid electrolyte interphase in Li-ion batteries. *Electrochimica Acta* **2010,** *55* (22), 6332-6341.

FIGURES

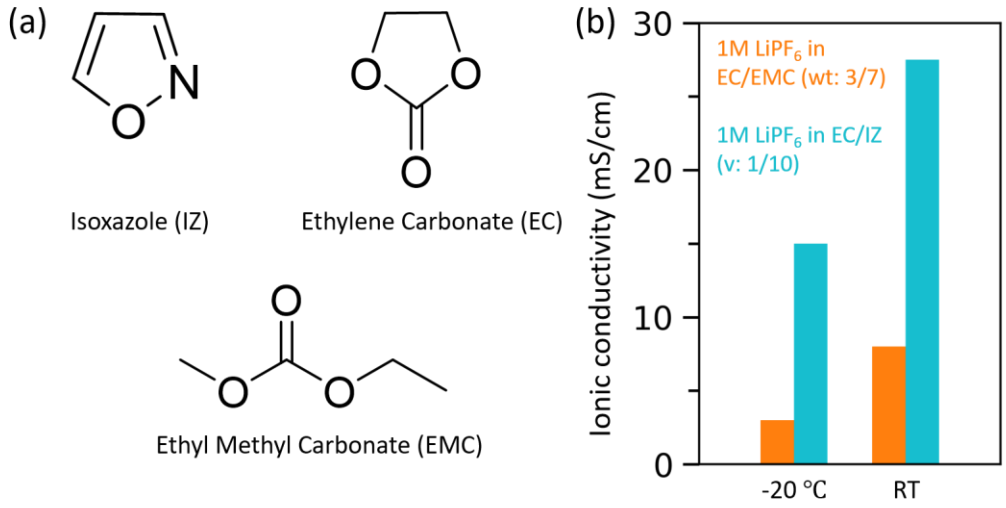

Figure 2-1. (a) Molecule structure of isoxazole, ethylene carbonate, ethyl methyl carbonate; (b) Ionic conductivity of 1M LiPF6 in EC/EMC (3/7, wt%) and 1M LiPF6 in EC/IZ (1/10, vol%) electrolytes at room temperature and -20°C.

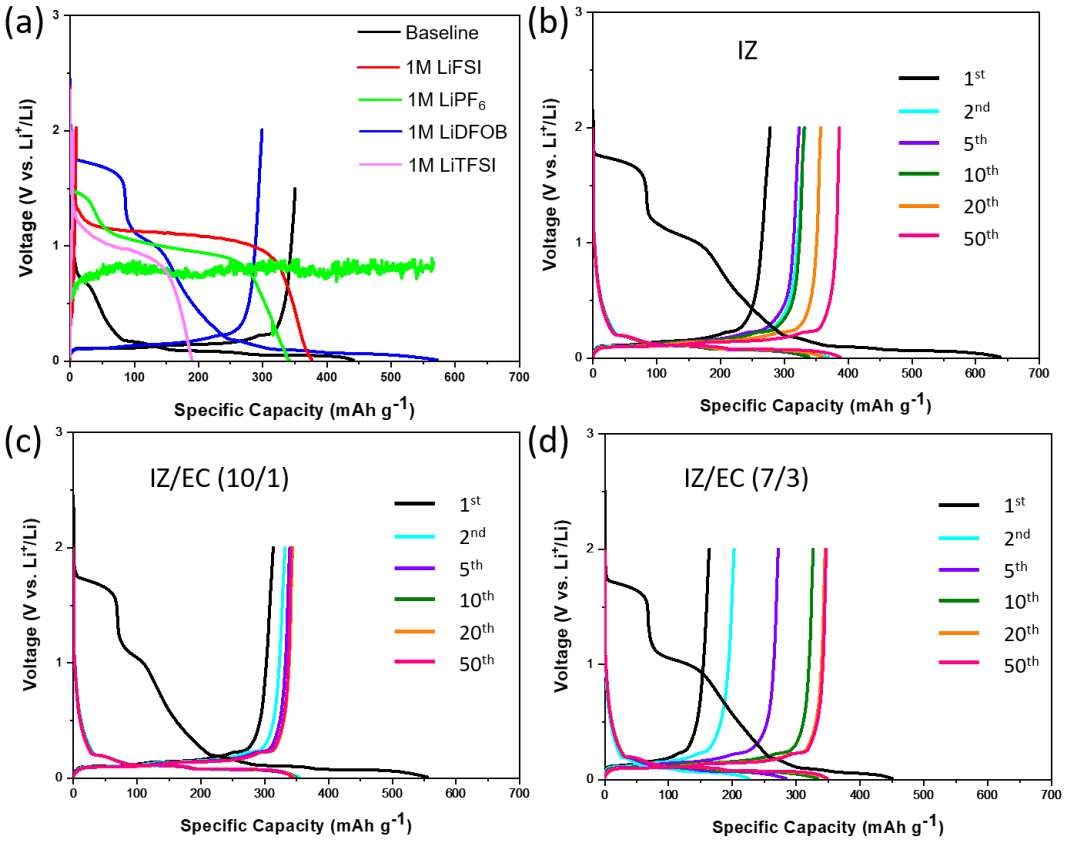

Figure 2-2. (a) First cycle charge/discharge curves of Li/graphite cells at room temperature using baseline (1M LiPF6 in EC/EMC), and isoxazole-based electrolytes with different salts.

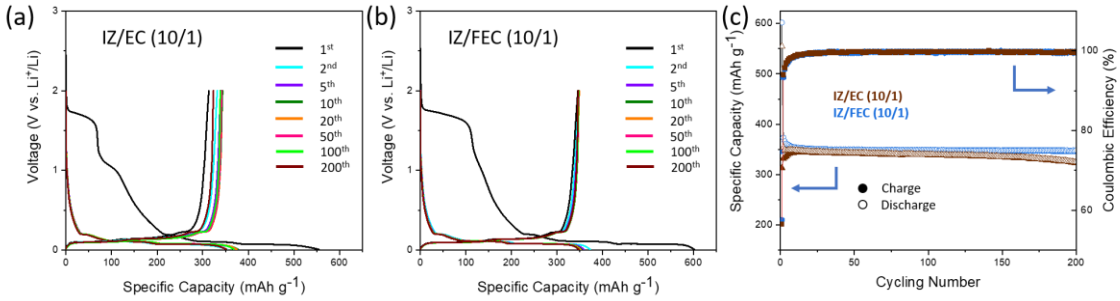

Figure 2-3. Charge/discharge curves of Li/graphite cells at room temperature using (a) 1M LiDFOB in isoxazole/EC (10/1, vol%); (b) 1M LiDFOB in isoxazole/FEC (10/1, vol%); (c) Long-term capacity retention and coulombic efficiency of Li/graphite cells using 1M LiDFOB in isoxazole/EC (brown), and 1M LiDFOB in isoxazole/FEC (blue) at room temperature.

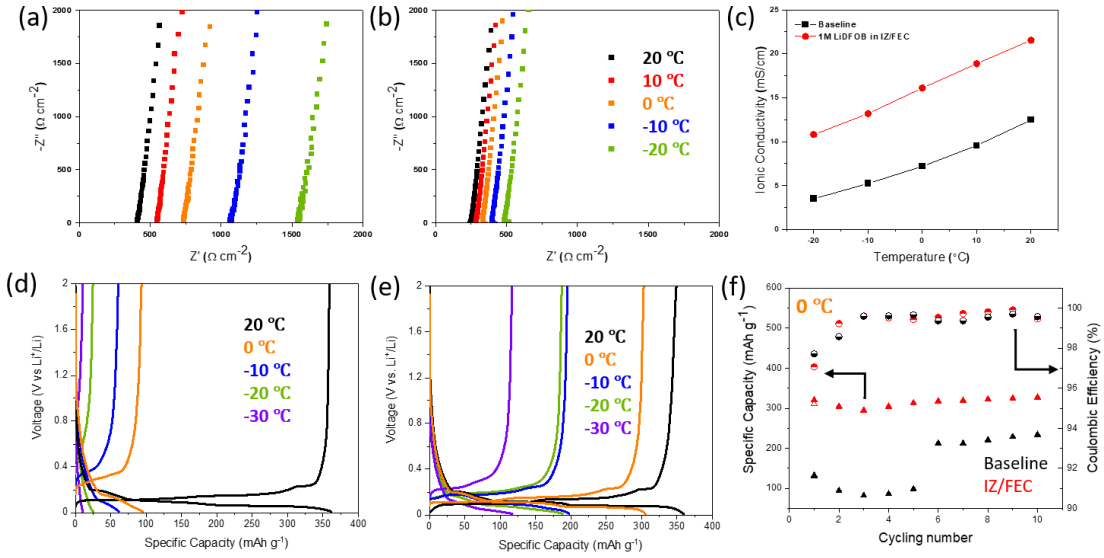

Figure 2-4. Electrochemical impedance spectroscopy (EIS) of (a) 1M $LiPF_6$ in EC/EMC (3/7) and (b) 1M LiDFOB in isoxazole/FEC (10/1, vol%) electrolytes at different temperatures. (c) Ionic conductivity of 1M $LiPF_6$ in EC/EMC (3/7) and 1M LiDFOB in isoxazole/FEC (10/1, vol%) electrolytes at different temperatures. Voltage profiles of Li/graphite cell using (d) 1M $LiPF_6$ in EC/EMC (3/7) and (e)1M LiDFOB in isoxazole/FEC (10/1, vol%) at various temperatures at C/10. (f) Cycling performance of Li/graphite cell using 1M $LiPF_6$ in EC/EMC (3/7) (baseline) and 1M DFOB in isoxazole/FEC (10/1, vol%) electrolytes at 0°C using C/10 rate.

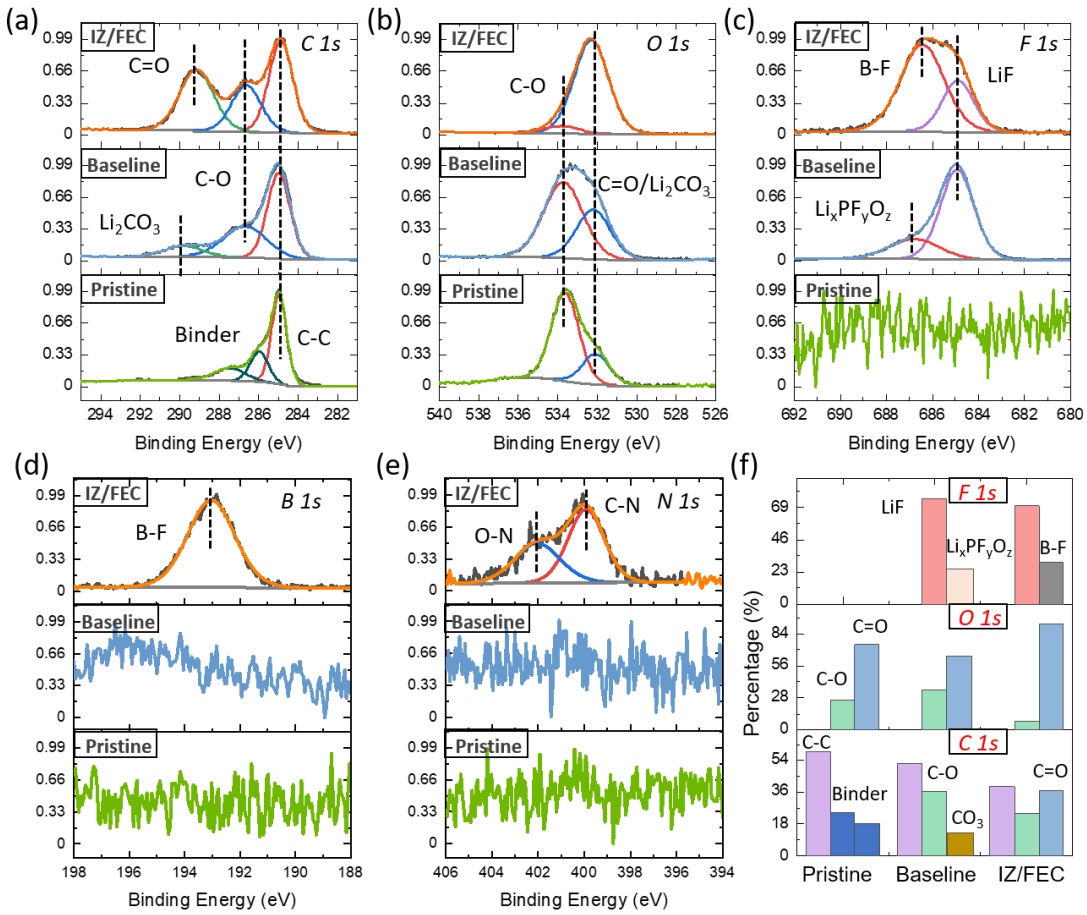

Figure 2-5. (a) C1s, (b) O1s, (c) F1s, (d) B1s and (e) N1s spectra of graphite electrode before (pristine) and after formation cycling using baseline and IZ/FEC electrolytes. (f) Calculated percent composition of the graphite surface species obtained from XPS measurement.

CHAPTER 3

Improved Low Temperature Performance of Graphite/Li Cells Using Isoxazole as a Novel Cosolvent in Electrolytes

Nuwanthi D. Rodrigo[1], Sha Tan[2], Zulipiya Shadike[2], Enyuan Hu[2], Xiao-Qing Yang[2], and Brett L. Lucht[1,†]

[1] Department of Chemistry, University of Rhode Island, Kingston, RI 02881, USA

[2] Chemistry Division, Brookhaven National Laboratory, Upton, NY 11973, USA

[†] *Corresponding author: blucht@uri.edu*

The following manuscript was published in the Journal of Electrochemical Society

ABSTRACT

An investigation of novel electrolyte formulations to improve low temperature performance of Li/graphite half cells has been conducted. A novel electrolyte co-solvent, isoxazole (IZ), has been investigated in electrolyte systems composed of lithium difluoro(oxalato)borate (LiDFOB) in fluoroethylene carbonate (FEC) and LiDFOB in ethylene carbonate (EC). Cells containing 1M LiDFOB FEC: IZ electrolyte have a significant improvement in capacity retention and reversible capacity at -10 ^{o}C. Ex-situ surface analysis of the cycled electrodes suggests that reduction of LiDFOB results in an oxalate rich solid electrolyte interphase (SEI). Addition of FEC, results in improved stability of the anode SEI preventing further decomposition of isoxazole solvent and improving cycling performance.

INTRODUCTION

Over the past few decades progress on the development of lithium-ion battery has led to lithium-ion batteries (LIB) becoming the most promising alternative to compete with internal combustion engines as a power source for vehicles. While there have been significant improvements in the energy and power density of LIB, more improvements in cost, cycle life and safety remain important. In addition, stable operation over a wide temperature range plays a critical role in the application of LIB for electric vehicles (EV), particularly at low temperatures. At temperatures below 0 ^{o}C, current commercial LIB have a significant decrease in reversible capacity and reduced performance.[1,2]

The electrolyte composition often plays a critical role in determining the operational temperature range for LIB.[3] Current LIB electrolytes contain ethylene carbonate (EC) as a critical component due to its unique ability to form a stable solid electrolyte interphase (SEI) on the graphite anode during initial formation cycling.[4] However, the high melting point (36.4 °C) of EC leads to increased viscosity and decreased Li^+ conductivity at low temperature.[5] Therefore, much effort has been made to improve low temperature performance of LIB by developing novel electrolyte systems with favorable physical properties such as low melting point, low viscosity, and high ionic conductivity at low temperature.[6,7]

In commercial LIB, graphite is the prominent choice of anode material, due to low cost, moderate capacity, and excellent cycle life.[8] However, graphite is well known for its poor electrochemical performance at subzero temperature. Formation of a solid electrolyte interphase (SEI) layer on the graphite is unavoidable since the working potential of the graphite electrode lies beyond the thermodynamic stability window of typical carbonate-based LIB electrolytes.[3,5,9] The composition and morphology of the SEI layer generated on

graphite depends on the electrolyte composition and the operating conditions.[10–12] The nature of the SEI plays a key role in the Li^+ intercalation kinetics and thus affect the performance of not only the graphite anode but also the entire cell.[13,14] It has been widely reported in the literature that increased charge transfer resistance at the electrode/electrolyte interphase as well as the rate of solid-state Li^+ diffusion in the bulk electrode are known to contribute to reduced performance at low temperature.[15–17] Therefore, properties of the SEI formed on graphite surface have a strong influence on the low temperature performance of LIBs.

In an effort to improve the low temperature performance of LIB, novel electrolyte formulations that form a stable SEI on the graphite anode with good lithium-ion transport properties have been investigated. Incorporation of isoxazole (IZ) as a novel cosolvent in electrolyte systems composed of lithium difluoro(oxalato)borate (LiDFOB) in fluoroethylene carbonate (FEC) and LiDFOB in ethylene carbonate (EC) have been investigated in Li/graphite half cells at low temperature. Improved electrochemical performance was observed in cells containing 1M LiDFOB in FEC: IZ at -10 °C. To better understand the source of enhanced performance, ex-situ surface analysis of anode surface films has been conducted via X-ray photoelectron spectroscopy (XPS) and infra-red with attenuated total reflectance (IR-ATR) after both formation cycling and long-term cycling.

EXPERIMENTAL

Graphite anodes (94.5% active material, 8 mg/cm^2 active material loading and 5.5% conductive carbon and SBR+CMC binder) and Li metal chips (16 mm) were purchased from MTI Corporation. Battery grade solvents ethylene carbonate (EC), fluoroethylene carbonate (FEC) and battery grade salt lithium difluoro(oxalato)borate (LiDFOB) were

obtained from BASF (Germany). Battery grade ethyl methyl carbonate (EMC) was obtained from Gotion (USA). 99% pure Isoxazole (IZ) was purchased from Sigma-Aldrich. All the reagents were stored in an Ar filled glove box and were used without further purification.

The graphite electrodes were punched into 15 mm diameter disks and dried under vacuum overnight at 110 °C prior to cell assembly. Coin cells (CR2032) were assembled in an Ar filled glove box (M-Braun) with oxygen and water contents <1 ppm. Two-electrode configuration cells were constructed with a 15 mm graphite working electrode, a Celgard 2325 separator (19mm), a Whatman GFD microfiber separator (15.6 mm), a 16 mm lithium chip counter electrode, and 100 µl of electrolyte. Electrolytes investigated include 1.2 M $LiPF_6$ in EC: EMC (3:7) obtained from BASF (standard electrolyte, STD), and isoxazole (IZ) based electrolyte formulations namely; 1 M LiDFOB in FEC: IZ 1:9 (v:v) and 1 M LiDFOB in EC:IZ 1:9 (v:v).

All the cell cycling was carried out with an Arbin LBT21084 high precision battery cycler. Fabricated coin cells were charged (lithiated) and discharged (delithiated) within a voltage range of 0.005 V and 1.5 V. The cells were cycled with the following procedure: Cells were cycled for 5 cycles at 25 °C with a current corresponding to C/10 between 1.5 V and 0.005 V and voltage was held at 0.005 V at the top of charge until the current dropped below C/20. After the initial five formation cycles, the cells were cycled at a C/10 current having a taper charge step at 0.005 V at the top of charge for 10 minutes for 5 cycles each at 25 °C, 0 °C and -10 °C, respectively. After low temperature cycling, cells were cycled at 25 °C for another 10 cycles at the same current rate of C/10 with a 10 minute taper charge step at 0.005 V at end of the charge cut off voltage. For the low-temperate charge/discharge test,

after charging at room temperature, cells were placed in a Tenney environmental chamber at the desired temperature (+/- 1°C) for 10 hours for temperature equilibration. Multiple cells for each electrolyte formulation were tested to confirm the reproducibility. Representative data is presented.

After completing the formation cycling and long-term cycling (low temperature cycling and post-low temperature cycling at 25 °C) cells were dissembled in an Ar-glove box. Delithiathed graphite electrodes extracted from the cells were rinsed with 3×500µl anhydrous dimethyl carbonate (99+%, Acros, DMC) to removal residual electrolyte and dried under vacuum overnight. X-ray photoelectron spectroscopy (XPS) measurements were acquired with a Thermo K-alpha system using Al Kα radiation (hυ=1486.6 eV) under ultra-high vacuum conditions ($<1\times10^{-12}$atm) with a measured spot size of 400 µm. Samples were transferred into the XPS chamber with a vacuum transfer vessel to avoid exposure to air. The binding energy was corrected based on the C 1s of C-C at 285.0 eV. Infra-red with attenuated total reflectance (IR-ATR) spectra of graphite electrodes were obtained on a Bruker Tensor 27 spectrometer, using a Pike MIRacle horizontal ATR accessory equipped with a germanium crystal in a nitrogen-filled glovebox. All spectra were collected with 512 scans at spectral resolution of 4 cm^{-1}. An atmospheric compensation and baseline correction were applied to all spectra.

RESULTS AND DISCUSSION

Electrolyte formulations based on isoxazole (IZ) (figure 3-1) as a cosolvent and lithiumdifluoro(oxalato)borate (LiDFOB) as lithium salt was investigated for improving the low temperature cycling performance of Li/graphite half cells. For this investigation two electrolyte formulations which have been recently developed, 1M LiDFOB in FEC: IZ

(1:9 v/v) and 1M LiDFOB in EC: IZ (1:9 v/v) have been selected.[18] A carbonate electrolyte, 1.2 M $LiPF_6$ in EC: EMC (STD) was selected as the baseline electrolyte formulation. All cycling was carried out in 2032 type coin cells according to the procedure described in the experimental section.

Specific capacity vs cycle number and columbic efficiency vs cycle number for the electrolytes investigated at different temperatures (25 °C, 0 °C and -10 °C) are provided in Figure 3-2(a) and Figure 3-2(b) respectively. As shown in Figure 3-2 (a), over the first 10 cycles at 25 °C cells with the STD electrolyte formulation have similar reversible capacity, ~365 mAh/g, as of the cells with 1M LiDFOB in FEC: IZ and 1M LiDFOB in EC: IZ electrolyte systems. After 5 cycles at 0 °C, the 1M LiDFOB FEC: IZ electrolyte has a better capacity retention (74%) compared to both the STD and 1M LiDFOB in EC: IZ electrolytes which had a capacity retention of 43% and 48 %, respectively. As the temperature is further lowered to -10 °C, the capacity of the STD and 1M LiDFOB in EC: IZ electrolytes drops below 50 mAh/g while the 1M LiDFOB in FEC: IZ electrolyte has a stable reversible capacity of 155 mAh/g. In the IZ based electrolyte systems, improved cycling performance is observed when EC is replaced by FEC due to the formation of a stable SEI as a result of FEC reduction on the surface of the graphite anode.[19–21] After low temperature cycling, cells are returned to room temperature to investigate capacity retention. A slightly decreased capacity retention is observed for cells containing the STD electrolyte formulation suggesting that unwanted lithium plating may have occurred during low temperature cycling of these cells.[22]

Coulombic efficiencies of the cells with STD, 1M LiDFOB in EC: IZ and 1M LiDFOB in FEC: IZ are presented in Figure 3-2(b). The first cycle efficiency for the cells with the STD

formulation is higher than the cells with 1M LiDFOB in EC: IZ and 1M LiDFOB in FEC: IZ. However, after the formation cycles all the electrolyte formulations have similar efficiencies of 99.5%.

The 1st cycle differential capacity vs voltage plot for coin cells built with 1.2 M $LiPF_6$ in EC: EMC (STD) and 1M LiDFOB in IZ with FEC and EC is provided in Figure 3-3. Cells built with the STD electrolyte contain a peak around 0.6 V vs Li/Li^+ in the dq/dv plot. As previously reported, this peak results from the reduction of EC on the surface of graphite.[23] Cells containing the 1M LiDFOB in EC: IZ and 1M LiDFOB in FEC: IZ electrolyte contains a large dominant peak around 1.65 V vs Li/Li^+ which has been reported in literature for the reduction of LiDFOB on the anode surface.[24] A small peak around 1-1.1 V vs Li/Li^+ is observed for both IZ based electrolyte formulations and is believed to result from reduction of isoxazole. Reduction of isoxazole on the graphite surface suggests that the SEI layer formed by LiDFOB on graphite during 1st cycle is unable to fully passivate the surface and the formulation needs to be modified to prevent the reduction of isoxazole. Addition of FEC as a cosolvent in 1M LiDFOB in FEC: IZ formulation suppresses the isoxazole reduction peak, suggesting that the reduction of FEC may result in the generation of a stable SEI on graphite which could prevent isoxazole reduction. The reduction of FEC has been previously reported to generate polycarbonate and LiF.[25] The presence of the combination of polycarbonate and LiF has been suggested to stabilize the SEI and inhibit the decomposition of the SEI components. Similar trends are discussed below.

In order to evaluate the origin of improved cycling performance, the surface film formed on graphite electrodes has been investigated by XPS after formation cycling and after long term cycling. The C1s, O1s, F1s, B1s and N1s spectra of a pristine graphite electrode and

graphite electrodes after formation cycling in STD, 1 M LiDFOB in FEC: IZ and 1M LiDFOB in EC: IZ are presented in figure 3-4. The C1s spectra of the pristine graphite electrode contains a high intensity peak characteristic of C-C/C-H at 285 eV along with CO_x peaks at 286.7 eV and 288.1 eV characteristic to CMC binder.[26] XPS spectra of graphite electrodes after formation cycling with STD electrolyte reveal the appearance of new C1s peaks characteristic of lithium alkyl carbonates and lithium carbonate at 290 eV. These peaks have been previously reported as reductive decomposition products of carbonate solvents from SEI formation.[27,28]

XPS spectra of the anode surface films of 1M LiDFOB in FEC: IZ and 1M LiDFOB in EC: IZ are significantly different from the surface film generated from the STD electrolyte. However, the XPS spectra of 1M LiDFOB in FEC: IZ and 1M LiDFOB in EC: IZ are similar. This suggests that the SEI formed in both IZ based electrolytes is dominated by the reduction products of LiDFOB. The C1s peaks at 289.1 eV (C=O) and 286.8 eV (C-O) are characteristics of oxalates from the reduction of LiDFOB, as previously reported.[29,30] A broad peak centered around 533 eV is observed in the O1s spectrum consistent with a mixture of (C=O) and (C-O) containing species. The F1s spectra contain two peaks characteristic of LiF at 685 eV and a B-F containing species at ~687 eV consistent with previously reported reduction products of LiDFOB.[31,32] Differences in relative peak ratio of LiF to B-F containing species are similar for the two IZ-based electrolytes, although the 1M LiDFOB in EC: IZ electrolyte has slightly more LiF and less B-F while the 1M LiDFOB in FEC: IZ electrolyte has slightly more B-F and less LiF. The B1s spectra of IZ-based formulations further supports the decomposition of LiDFOB in SEI formation. The corresponding peaks characteristic of B-F and B-O are found in the B1s spectrum around

192.5-193.8 eV.[30,31] The appearance of N1s peaks in both IZ-based formulations suggests reduction of isoxazole during SEI formation, which is consistent with the observed isoxazole reduction peak at 1.1 V in the dq/dv plot in Figure 3.

Relative atomic concentrations of elements detected on the graphite electrode after formation cycling with STD and IZ-based electrolyte formulations along with the fresh electrode are provided in Figure 3-5a. After the formation cycles, anodes extracted from STD have a decrease in the C concentration and increase in O and F concentrations. A similar trend in elemental concentrations is observed for IZ-based electrolytes having a decrease in C concentration and increase in O, F, B and N concentrations. The higher O concentration and lower F concentration suggest the decomposition of LiDFOB salt is the major SEI forming reduction reaction in IZ-based electrolyte. In addition, reduction of isoxazole also occurs on the graphite anode which is supported by a low concentration of N. However, introduction of FEC or EC as a cosolvent do not significantly alter the SEI composition. As depicted in Figure 3-3, upon decreasing the potential during lithiation, reduction of LiDFOB occurs on the surface of the anode at 1.65 V vs Li prior to the reduction of FEC or EC, forming an initial SEI rich in oxalates and borates. This is supported by both the XPS element spectra, and the atomic concentrations of both anodes cycled with the IZ-based electrolytes. The changes in the atomic concentrations for all the electrolyte formulations are consistent with generation of SEI on the anode as previously reported.

The C1s, O1s, F1s, B1s and N1s XPS spectra of anodes after long term cycling are provided in Figure 3-6. Upon extended cycling with the STD electrolyte, significant changes in the XPS element spectra observed are consistent with an evolution and thickening of the

SEI.[33,34]

Alternatively, the XPS spectra of the graphite electrodes cycled with IZ-based electrolytes are largely unchanged upon extended cycling. Increased thickness of the SEI on the graphite electrode cycled with the STD electrolyte is supported by the decreased intensity of C-C peak (285 eV) and increased intensities of the C-O (287 eV) and C=O (289 eV) peaks in the C1s spectrum.[23] The broadening of the O1s XPS spectrum is also consistent with additional electrolyte decomposition upon extended cycling with STD electrolyte. In addition to electrolyte decomposition peaks, the presence of a lithiated graphite C1s peak at 282.5 eV is consistent with residual lithiated graphite, suggesting sluggish Li^+ intercalation/deintercalation kinetics at the electrolyte/electrode interface in STD electrolyte system.[35] Significant changes in the elemental concentration of C, O and F for graphite anodes cycled with the STD electrolyte provide additional support for an evolution and thickening of the SEI upon extended cycling. The XPS element spectra of graphite electrodes extracted from 1M LiDFOB in FEC: IZ are similar to the element spectra of 1M LiDFOB in EC: IZ. The XPS results suggest that the surface films formed from the IZ-based electrolytes have only small changes to the SEI after extended cycling. The F1s spectra

have an increase for the peak characteristic of B-F species (687 eV) upon prolonged cycling, which is also supported by changes in the elemental concentrations provided in Figure 3-5b. After extended cycling, the surface films generated from IZ-based electrolytes are still dominated by oxalates from the reduction of LiDFOB as evidenced by peaks characteristic of C-O (286.8 eV) and C=O (289.1 eV) in the C1s spectra and a complementary broad peak centered at 533 eV in the O1s spectra.[30,31] The presence of a

B1s peak at 193 eV further supports LiDFOB reduction on anode surface for the IZ-based electrolytes. Overall, cells cycled with IZ-based electrolytes have a stable SEI dominated by LiDFOB reduction products while the cell cycled with the STD electrolyte has an SEI dominated by EC and $LiPF_6$ reduction products.

IR-ATR spectra of graphite electrodes acquired after formation cycling and after long-term cycling for the STD, 1M LiDFOB FEC: IZ and 1M LiDFOB EC: IZ electrolytes are provided in Figure 3-7. The IR spectra of anodes extracted from cells cycled with the STD electrolyte contain a strong absorption peak at 1660 cm^{-1} characteristic of lithium alkyl carbonates, most likely from lithium ethylene dicarbonate (LEDC) previously reported as the reduction product of EC.[28,31] In addition, absorption peaks are observed at 1555 cm^{-1} and 1540 cm^{-1} characteristics of Li_2CO_3.[32] There are no significant changes in the IR spectra for anodes extracted from cells after extended cycling with the STD electrolyte, consistent with an SEI dominated by LEDC and Li_2CO_3.

The IR spectra of the graphite electrodes cycled with IZ-based electrolytes are significantly different than the IR spectra of the graphite electrodes cycled with the STD electrolyte, but similar to each other. New absorption peaks are observed in IZ-based electrolytes containing LiDFOB at 1800 cm^{-1} and 1758 cm^{-1}. The observed new peaks in C=O stretching region are characteristic of in phase and out of phase oscillations of the two carbonyl groups present in oxolatoborates.[29,36] In addition, strong absorptions are observed at 1635 cm^{-1} characteristic of lithium oxalates or other oxalate containing species. IR absorptions are also observed at 1660 cm^{-1} consistent with the presence of lithium alkyl carbonates and at 1555 cm^{-1} and 1540 cm^{-1} characteristic of Li_2CO_3.[32] However, upon long-term cycling the IR absorptions characteristic of Li_2CO_3 are decreased in the 1M LiDFOB

EC: IZ electrolyte and completely disappear in the 1M LiDFOB in FEC: IZ electrolyte. Interestingly, the relative intensity of the lithium alkyl carbonate and oxalate peaks increases upon cycling in 1M LiDFOB FEC: IZ electrolyte.

Combination of XPS and IR analysis provides significant information into the composition of the SEI generated from the different electrolytes. The differences in surface chemistry for cells cycled with IZ-based electrolytes likely result from the reduction of LiDFOB. Generation of a stable SEI rich with oxalates and oxalatoborates prevents further electrolyte degradation upon further cycling. Whereas the SEI in STD electrolyte is dominated by lithium alkyl carbonates and continuous electrolyte decomposition during cycling results in the generation of a thicker surface film on the graphite.

CONCLUSIONS

Isoxazole based novel electrolyte systems containing LiDFOB have been investigated to improve low temperature cycling performance of graphite/Li half cells. Compared to standard carbonate electrolytes, IZ-based electrolytes containing FEC, or EC have improved performance at low temperature. In particular, 1M LiDFOB in FEC: IZ has outstanding cycling performance at -10 °C having a stable reversible capacity of 150 mAh/g. Ex-Situ surface analysis of graphite anodes reveals the surface chemistry of the anodes in IZ-based electrolytes is dominated by oxalates and the surface composition does not significantly change upon cycling. The surface composition of anode cycled with the STD electrolyte evolves over cycling, resulting in the formation of a thick SEI. The nature and the composition of the SEI are believed to play a key role in determining low temperature cycling performance of the electrolytes investigated. The presence of oxalates from LiDFOB reduction from IZ-based electrolytes improves the SEI stability and low temperature cycling performance.

ACKNOWLEDGMENT

This work was supported by the Assistant Secretary for Energy Efficiency and Renewable Energy, Vehicle Technology Office of the U.S. DOE through Applied Battery Research for Transportation (ABRT) program under contract No. DE-SC0012704.

REFERENCES

1. M. C. Smart, B. V. Ratnakumar, K. B. Chin, and L. D. Whitcanack, *Journal of The Electrochemical Society*, **157**, A1361–A1373 (2010).

2. S. Herreyre, O. Huchet, S. Barusseau, F. Perton, J. M. Bodet, and Ph. Biensan, *Journal of Power Sources*, **97**–**98**, 576–580 (2001).

3. K. Xu, *Chemical Reviews*, **104**, 4303–4417 (2004).

4. D. Aurbach, Y. Ein-Eli, B. Markovsky, A. Zaban, S. Luski, Y. Carmeli, and H. Yamin, *Journal of The Electrochemical Society*, **142**, 2882–2890 (1995).

5. K. Xu, *Chemical Reviews*, **114**, 11503–11618 (2014).

6. E. R. Logan, E. M. Tonia, K. L. Gering, J. Li, X. Ma, L. Y. Beaulieu, and J. R. Dahn, *Journal of The Electrochemical Society*, **165**, A21–A30 (2018).

7. Q. Li, S. Jiao, L. Luo, M. S. Ding, J. Zheng, S. S. Cartmell, C.-M. Wang, K. Xu, J.-G. Zhang, and W. Xu, *ACS Applied Materials and Interfaces*, **9**, 18826–18835 (2017).

8. R. Wagner, N. Preschitschek, S. Passerini, J. Leker, and M. Winter, *Journal of Applied Electrochemistry*, **43**, 481–496 (2013).

9. L. Xing, X. Zheng, M. Schroeder, J. Alvarado, A. von Wald Cresce, K. Xu, Q. Li, and W. Li, *Accounts of Chemical Research*, **51**, 282–289 (2018).

10. D. Aurbach, B. Markovsky, I. Weissman, E. Levi, and Y. Ein-Eli, *Electrochimica Acta*, **45**, 67–86 (1999).

11. D. Aurbach, *Journal of Power Sources*, **89**, 206–218 (2000).

12. S. J. An, J. Li, C. Daniel, D. Mohanty, S. Nagpure, and D. L. Wood III, *Carbon*, **105**, 52–76 (2016).

13. C.-K. Huang, J. S. Sakamoto, J. Wolfenstine, and S. Surampudi, *Journal of The Electrochemical Society*, **147**, 2893 (2000).

14. T. R. Jow, S. A. Delp, J. L. Allen, J.-P. Jones, and M. C. Smart, *Journal of The Electrochemical Society*, **165**, A361–A367 (2018).

15. S. S. Zhang, K. Xu, and T. R. Jow, *Electrochimica Acta*, **48**, 241–246 (2002).

16. S. S. Zhang, K. Xu, and T. R. Jow, *Journal of Power Sources*, **115**, 137–140 (2003).

17. B. P. Matadi, S. Geniès, A. Delaille, C. Chabrol, E. de Vito, M. Bardet, J.-F. Martin, L. Daniel, and Y. Bultel, *Journal of The Electrochemical Society*, **164**, A2374–A2389 (2017).

18. S. Tan, U. N. D. Rodrigo, Z. Shadike, B. Lucht, K. Xu, C. Wang, X.-Q. Yang, and E. Hu, *ACS Applied Materials & Interfaces*, **13**, 24995–25001 (2021).

19. E. Markevich, G. Salitra, and D. Aurbach, *ACS Energy Letters*, **2**, 1337–1345 (2017).

20. N. von Aspern, G. V. Röschenthaler, M. Winter, and I. Cekic-Laskovic, *Angewandte Chemie - International Edition*, **58**, 15978–16000 (2019).

21. Z. L. Brown, and B. L. Lucht, *Journal of The Electrochemical Society*, **166**, A5117–A5121 (2019).

22. J. Wandt, P. Jakes, J. Granwehr, R. A. Eichel, and H. A. Gasteiger, *Materials Today*, **21**, 231–240 (2018).

23. M. Nie, J. Demeaux, B. T. Young, D. R. Heskett, Y. Chen, A. Bose, J. C. Woicik, and B. L. Lucht, *Journal of The Electrochemical Society*, **162**, A7008–A7014 (2015).

24. Z. Chen, J. Liu, and K. Amine, *Electrochemical and Solid-State Letters*, **10**, 45–48 (2007).

25. A. L. Michan, B. S. Parimalam, M. Leskes, R. N. Kerber, T. Yoon, C. P. Grey, and B. L. Lucht, *Chemistry of Materials*, **28**, 8149–8159 (2016).

26. L. El Ouatani, R. Dedryvère, J.-B. Ledeuil, C. Siret, P. Biensan, J. Desbrières, and D. Gonbeau, *Journal of Power Sources*, **189**, 72–80 (2009).

27. M. Nie, D. Chalasani, D. P. Abraham, Y. Chen, A. Bose, and B. L. Lucht, *Journal of Physical Chemistry C*, **117**, 1257–1267 (2013).

28. D. M. Seo, D. Chalasani, B. S. Parimalam, R. Kadam, M. Nie, and B. L. Lucht, *ECS Electrochemistry Letters*, **3**, 91–94 (2014).

29. B. S. Parimalam, and B. L. Lucht, *Journal of The Electrochemical Society*, **165**, A251–A255 (2018).

30. M. Xu, L. Zhou, L. Hao, L. Xing, W. Li, and B. L. Lucht, *Journal of Power Sources*, **196**, 6794–6801 (2011).

31. M. Nie, and B. L. Lucht, *Journal of The Electrochemical Society*, **161**, A1001–A1006 (2014).

32. P. Verma, P. Maire, and P. Novák, *Electrochimica Acta*, **55**, 6332–6341 (2010).

33. S. K. Heiskanen, J. Kim, and B. L. Lucht, *Joule*, **3**, 2322–2333 (2019).

34. M. Herstedt, D. P. Abraham, J. B. Kerr, and K. Edström, *Electrochimica Acta*, **49**, 5097–5110 (2004).

35. N. Ehteshami, L. Ibing, L. Stolz, M. Winter, and E. Paillard, *Journal of Power Sources*, **451**, 227804 (2020).

36. G. V. Zhuang, K. Xu, T. R. Jow, and P. N. Ross, *Electrochemical and Solid-State Letters*, **7**, A224–A227 (2004).

FIGURES

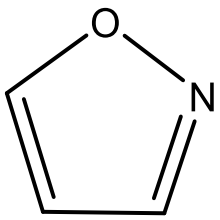

Figure 3-1. Chemical structure of Isoxazole (IZ)

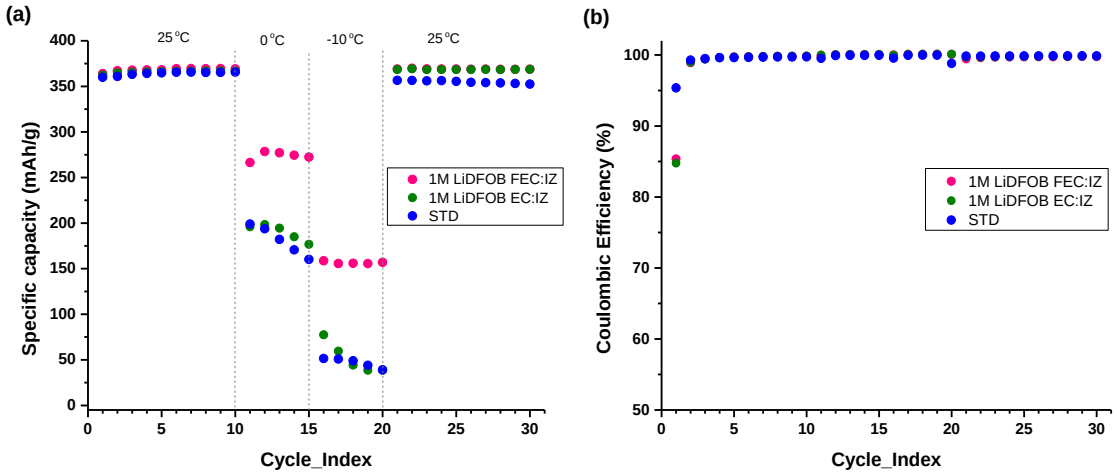

Figure 3-2. Specific capacity vs. cycle number (a), and Coulombic efficiency vs. cycle number (b) for Graphite/Li half cells using STD electrolyte (in blue), 1M LiDFOB FEC: IZ (in pink) and 1M LiDFOB EC: IZ (in green).

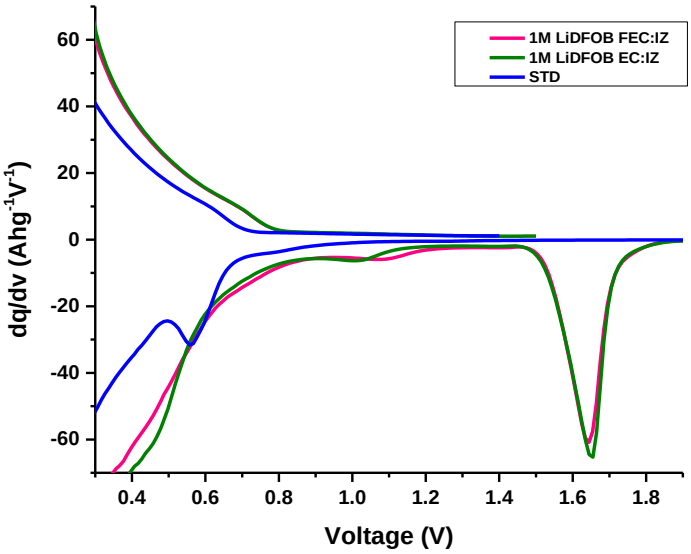

Figure 3-3. 1st cycle dq/dv plot for Graphite/Li half cells using STD electrolyte (in blue), 1M LiDFOB FEC: IZ (in pink) and 1M LiDFOB EC: IZ (in green)

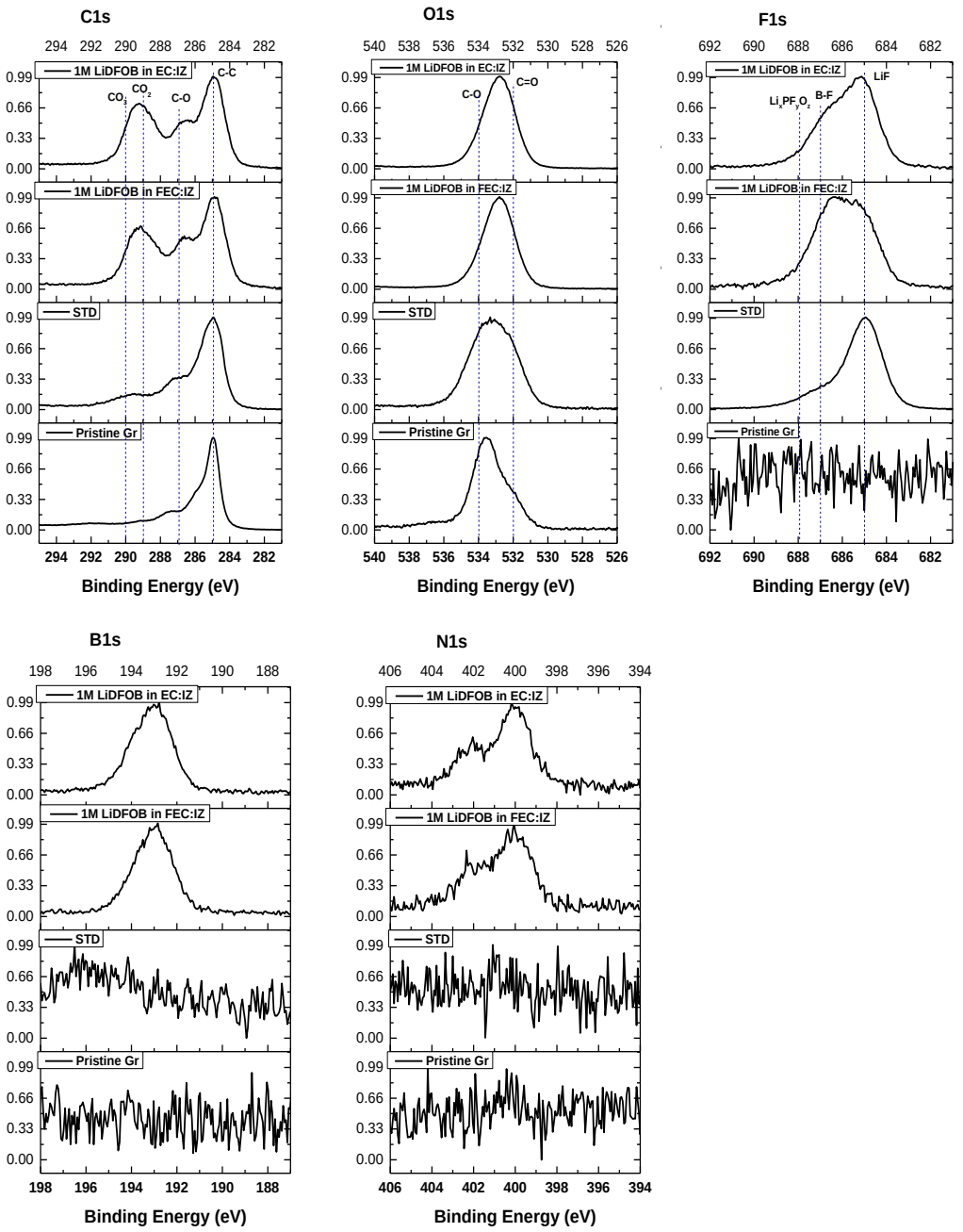

Figure 3-4. C1s, O1s, F1s, N1s and B1s spectra of graphite anodes after formation cycling.

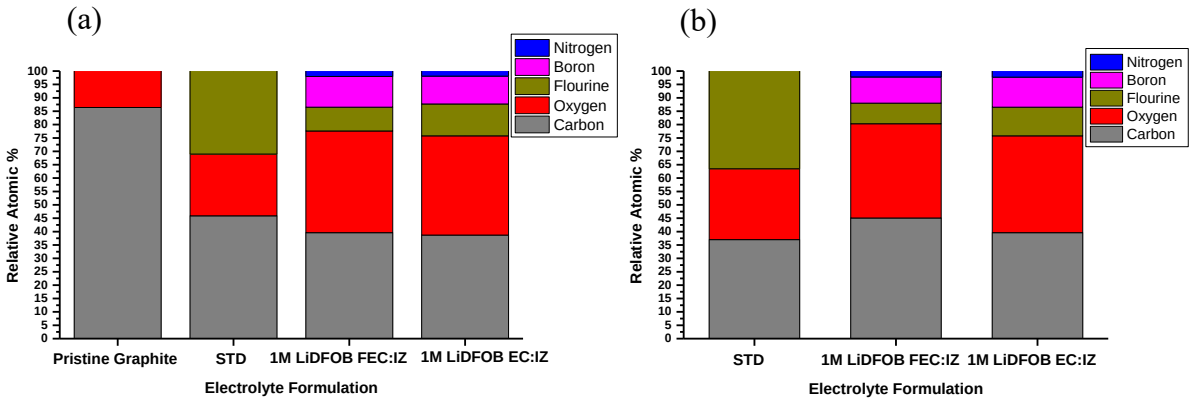

Figure 3-5. Corresponding relative atomic concentrations from XPS elemental spectra obtained for graphite anodes (a) after formation and (b) at the end of testing.

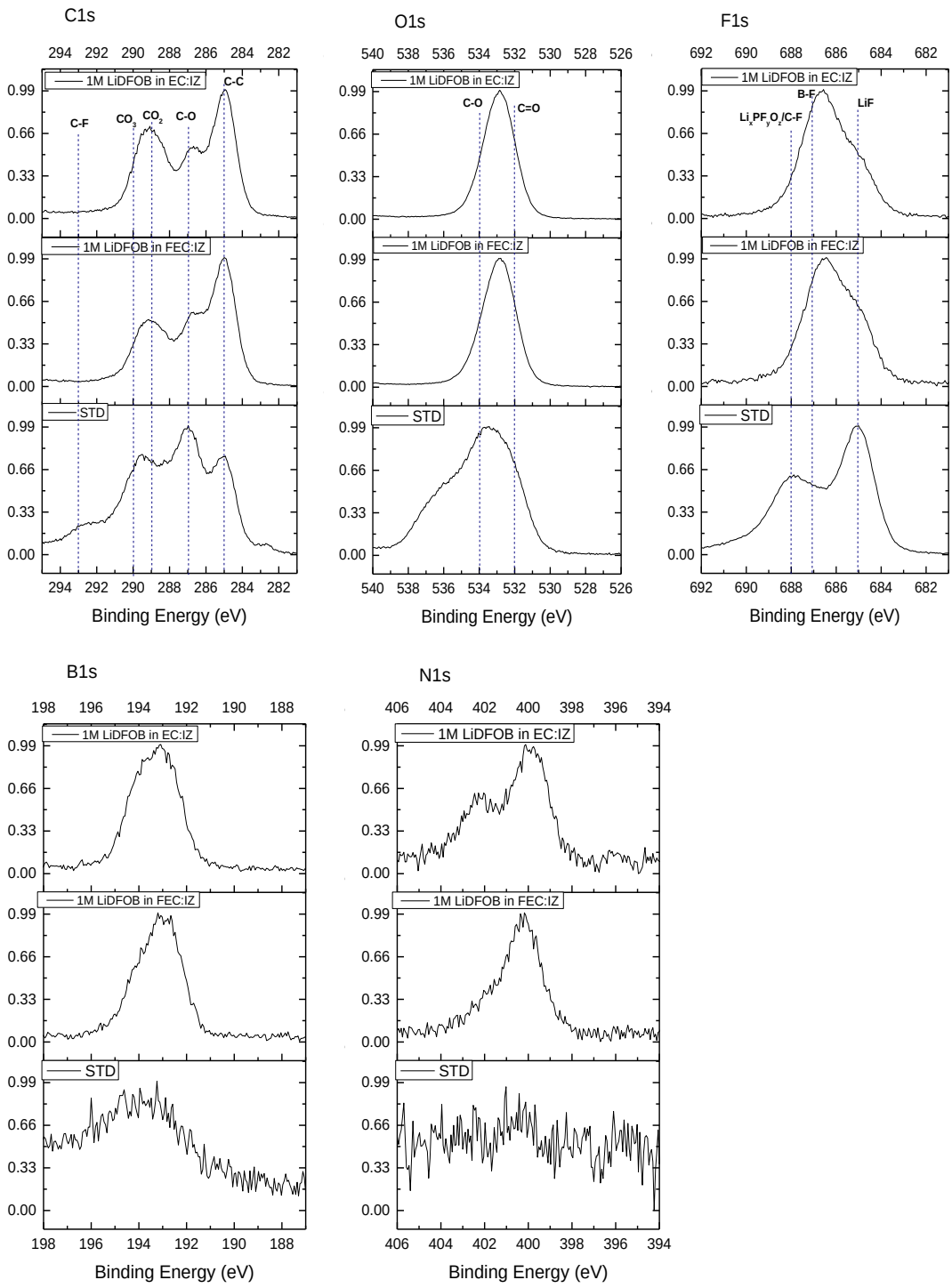

Figure 3-6. C1s, O1s, F1s, N1s and B1s spectra of graphite anodes at the end of testing.

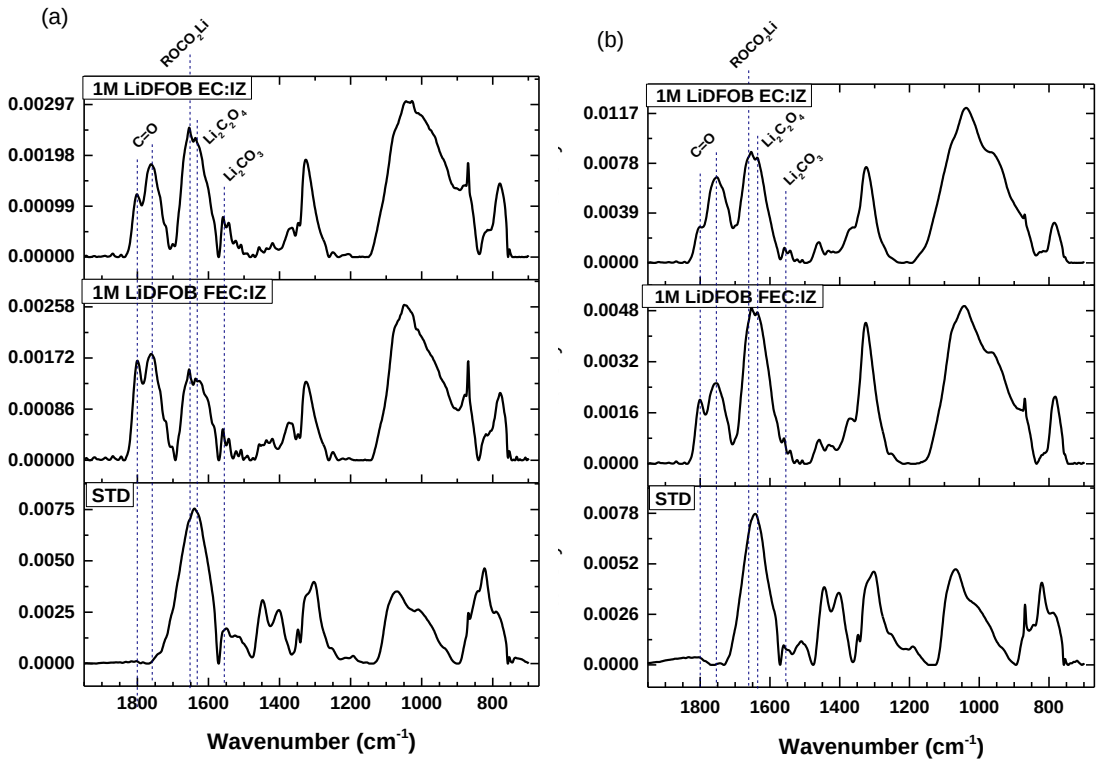

Figure 3-7. IR-ATR spectra of graphite anodes (a) after formation and (b) at the end of testing

CHAPTER 4

Investigation of the electrode- electrolyte interphase in ester-based electrolytes in NCM523/graphite cells

Nuwanthi D. Rodrigo[1], Chamithri Jayawardana[1], and Brett L. Lucht[1,†]

[1] Department of Chemistry, University of Rhode Island, Kingston, RI 02881, USA

† Corresponding author: blucht@uri.edu

The following manuscript has been submitted for review in the Journal of the Electrochemical Society

ABSTRACT

The use of methyl acetate (MA) and methyl propionate (MP) as co-solvents in carbonate/$LiPF_6$ electrolytes have been investigated in $LiNi_{0.5}Co_{0.2}Mn_{0.3}O_2$ (NCM523)/graphite cells to improve electrochemical performance at low temperature (-20 ˚C). Consistent with previous investigations, improved low temperature performance was observed with all electrolyte formulations containing esters. Detailed *ex-situ* surface analysis of the surface films generated with the ester-based electrolytes containing electrolyte additives reveal significant changes to the SEI on graphite upon cycling at moderately elevated temperature (45 ˚C). In the presence of vinylene carbonate (VC) lithium plating is observed upon cycling at low temperature (-20 ˚C) which leads to a thicker solid electrolyte interface (SEI) upon cycling at 45 ˚C. Incorporation of fluoroethylene carbonate (FEC) as an electrolyte additive result in the generation of a thin SEI and alters the structure of the surface film on the NCM523 cathode resulting in stable cycling over a wide temperature range.

INTRODUCTION

Over the past few decades, lithium-ion batteries have been extensively investigated as energy storage devices for applications ranging from consumer electronic to grid energy storage. Recent developments in increased energy and power density have made lithium-ion batteries the best candidate for powering electric vehicles (EVs). However, the performance of lithium-ion batteries is still limited by the operating temperature range, specially at subzero and moderately elevated temperatures.[1] It has been reported that poor electrochemical performance at low temperature is mainly attributed to increased lithium-ion transport resistance which originates from reduced ionic conductivity and increased viscosity of the electrolyte, increased charge transfer resistance at the electrode-electrolyte interface and decreased solid-state lithium ion diffusion in the graphite electrode.[2–4]

There have been numerous efforts reported in the literature to improve the performance over a wide operating temperature range mainly through adjusting the electrolyte composition. Formulating new electrolytes through the use of novel co-solvents, novel electrolyte additives, alternative lithium salts and optimized solvent blends have been reported to improve the low temperatures performance of lithium-ion batteries.[5–11] However, most of the electrolyte formulations developed to improve the low temperature performance are accompanied by decreases in capacity retention at moderately elevated temperatures. Therefore, formulating new electrolyte systems optimized for wide operating temperature range applications is challenging.

Carboxylate esters have been the most widely investigated co-solvents to improve the low temperature performance of lithium-ion batteries due to the favorable physicochemical properties and reasonable capacity retention at moderately elevated temperature.[12] Previous investigations suggest improved performance of lithium-ion batteries at low

temperature and improved rate capability at ambient temperature when esters are added as a co-solvent in carbonate based electrolyte formulations.[13–17] While extensive work has been reported for improving low temperature performance of carbonate electrolytes containing esters as co-solvents, there have been limited investigations of the electrode surface chemistry and the role of changes to the surface chemistry on the electrochemical performance of these electrolyte systems. Therefore, we report a detailed *ex-situ* analysis of the surface films generated on the anode and cathode in the presence of some of the best previously reported ester-containing electrolytes with and without FEC and VC as electrolyte additives for improving low temperature performance in lithium-ion batteries.[13,15]

EXPERIMENTAL

Single side coated graphite electrodes and $LiNi_{0.5}Co_{0.2}Mn_{0.3}O_2$ (NCM523) electrodes were purchased from MTI corporation with electrode compositions of 94.5 % active material, 8 mg/ cm^2 active material loading and 5.5% conductive carbon, sodium carboxymethyl cellulose and styrene butadiene rubber (CMC+ SBR) binders for graphite electrode, and 94.2% active material, 12.1 mg/cm^2 active material loading and 5.8% conductive carbon and polyvinylidene difluoride (PVdF) for NCM523 electrodes. Battery grade ethylene carbonate (EC), fluoroethylene carbonate (FEC), vinylene carbonate (VC) and battery grade lithium hexafluorophosphate ($LiPF_6$) were obtained from BASF (Germany). Battery grade ethyl methyl carbonate (EMC), methyl acetate (MA) and methyl propionate (MP) were supplied by Gotion (USA). All the chemical reagents were stored in an Ar filled glove box (M-Braun) and used without further purification.

2032-type coin cells were assembled with NCM523 positive electrodes (12.7 mm

diameter) and graphite negative electrodes (14 mm diameter), three separators [Celgard 2325 (19 ,15 mm in diameter), Whatman GF/D glass microfiber (15.6 mm in diameter)], and 100 μL of electrolyte solution in an argon glove box with oxygen and water contents < 1 ppm. Both NCM523 and graphite electrodes were dried at 110 °C under vacuum overnight before cell assembly. Electrolytes investigated include 1.2 M $LiPF_6$ in EC: EMC (3:7 vol %) (referred to as standard electrolyte, STD) from BASF.

Ester based electrolytes were prepared with MA and MP to make a stock solution of 1.2 M $LiPF_6$ in EC+EMC+MP (20:60:20 vol%) (MP electrolyte) and 1.2 M $LiPF_6$ in EC+EMC+MA (20:60:20 vol%) (MA electrolyte). Additives were then added to the stock MA and MP electrolyte solutions to achieve 2% concentration by volume for VC and FEC. The electrolyte formulations are listed in Table 4-1.

After assembly, cells were cycled at 25 ˚C for 5 formation cycles using a high precision battery cycler (Arbin LBT21084). The cells were cycled between 3- 4.2 V at a current density of C/20 in the first cycle, and a current of C/10 for 2^{nd} and 3^{rd} cycle, and a current density of C/5 for 4^{th} and 5^{th} cycle, respectively.

After formation cycling, the cells were cycled sequentially at different temperatures ranging from 25 ˚C, -20 ˚C, 25 ˚C to 45 ˚C. First, cells were cycled at a current corresponding to C/2 for 20 cycles at 25 ˚C. Then cells were transferred to a temperature chamber at -20 ˚C and cycled at a rate of C/5 for 5 cycles. After low temperature cycling, cells were placed in a temperature chamber at 25 ˚C and cycled for another 10 cycles at a C/2 rate. The cells were then transferred to a temperature chamber at 45 ˚C and cycled for 60 cycles at a C/2. At all temperatures, cells were cycled between a voltage of 3 – 4.2 V using a constant current-constant voltage (CC-CV) cycling mode with a C/20 cutoff at the

top of charge while for formation cycling CV step corresponding to 1/10 of the applied current of each C-rate at the top of charge. For low temperature charge/discharge testing, cells were placed in a Tenney environmental chamber at the desired temperature (+/- 1 ˚C) for 6 hours for temperature equilibration. It should be noted that, C-rates used at each temperature were decided based on initial rate study done on the coin cells constructed with MP containing electrolyte with and without two electrolyte additives. For each electrolyte formulation multiple cells were tested and representative data is presented.

For X-ray photoelectron spectroscopy (XPS), cells were dissembled in an Ar-glove box after formation cycling and after long-term cycling (at the end of cycling at 45 ˚C). Graphite and NCM 523 electrodes were extracted from fully discharged cells and extracted electrodes were rinsed with 3 x 500 µL of extra dry dimethyl carbonate (99+%, Acros, DMC) to remove residual electrolyte and dried under vacuum overnight. XPS measurements were acquired with a Thermo K-alpha system using Al Kα radiation (hυ=1486.6 eV) under ultra-high vacuum conditions ($<1\times10^{-12}$atm) with a measured spot size of 400 µm. Samples were transferred into the XPS chamber with a vacuum transfer vessel to avoid exposure to air. The binding energy was corrected based on the C 1s of C-C at 285.0 eV.

Infra-red with attenuated total reflectance (IR-ATR) spectra of graphite electrodes were obtained on a Bruker Tensor 27 spectrometer, using a Pike MIRacle horizontal ATR accessory equipped with a germanium crystal in a nitrogen-filled glovebox. All spectra were collected with 512 scans at spectral resolution of 4 cm^{-1}. An atmospheric compensation and baseline correction were applied to all spectra.

The morphology of the surface films on graphite electrodes were examined by Field-

emission scanning electron microscopy (FE-SEM). Graphite electrodes extracted from full cells at the end of 100 cycles were rinsed with DMC and then transferred to the SEM chamber (Zeiss SIGMA VP) with minimum air exposure. FE-SEM images were acquired using secondary electron detector (SE2) and accelerating voltage of 7 kV was used.

RESULTS AND DISCUSSION

The cycling performance of NCM523/graphite cells containing one of two esters, MP or MA, with and without VC and FEC as electrolyte additives over a wide operating temperature range [25 ˚C (RT), -20 ˚C and 45 ˚C] is provided in Figure 4-1. As presented in Figure 4-1, cells cycled with MP and MA have comparable specific capacities (~150 mAh/g) to cells cycled with STD electrolyte after initial formation cycles at RT whereas the cells cycled with either VC or FEC in both ester containing electrolytes have a slightly lower capacity of ~140 mAh/g. However, significant differences in cycling performance are observed upon cycling the cells at - 20 ˚C. Cells cycled in MP, MP+2% FEC and MP+2% VC have similar discharge capacities to each other, but all MP containing electrolytes outperformed the STD electrolyte. The highest capacity is observed for the MP+2% FEC electrolyte which is about 70 mAh/g. Alternatively, cells cycled with MA based electrolytes have a wide spread of capacities. The MA electrolyte has the highest capacity, 90 mAh/g, while the STD electrolyte has the lowest capacity of ~50 mAh/g. Overall, the MA electrolyte has the best capacity retention at -20 ºC for all the electrolyte formulations investigated.

After 5 cycles at low temperature all cells were returned to room temperature for 10 cycles. Cells cycled with all of the electrolyte formulations except MA+2% VC and MP+2% VC delivered their initial RT capacities. The decrease in the room temperate cycling capacities

for two ester electrolyte formulations containing VC as an electrolyte additive is most likely due to lithium plating on graphite electrode upon low temperature cycling.[17,18] The FE-SEM images (Figure 4-2e) support the presence of "filament like" and "granular shape" Li dendrite on the surface of graphite electrode cycled with MA+2% VC.[19] On contrary, there is no Li dendrite growth observed on the surface of the graphite electrode cycled with STD, MA and MA+2% FEC electrolytes. However, the deposition of thick surface films composed of electrolyte decomposition products are observed on the graphite electrode cycled with these electrolytes compared to pristine graphite electrode (Figure 4-2 a, b, c, d).

After RT cycling, cells were transferred to a temperature chamber at 45 ˚C and cycled for 60 cycles. Upon the elevated temperature cycling, a significant capacity fade was observed for the cells cycled with MA and MP electrolytes compared to the STD whereas a stable cycling was observed for the MA+ 2% FEC electrolyte. In addition, drastic capacity fade was observed for the cells cycled in MA+2% VC, most likely due to continuous electrolyte decomposition upon contact with the plated lithium on the anode surface.[17]Overall, at all the temperatures tested stable cycling performance was observed for cells with MA+2% FEC. The cells constructed and cycled with esters as co-solvents with and without the two electrolyte additives serves to verify and demonstrate the reproducibly of, low temperature and elevated temperature performance reported previously.[13–16]

Ex-situ surface analysis was performed after formation and long-term cycling to characterize the chemical composition of the surface films generated on both graphite and NCM523 electrodes extracted from graphite/NCM523 cells cycled with ester-based electrolytes. The C1s, O1s, F1s and P2p spectra of the surface films generated on the

graphite electrodes after formation cycling for MA based electrolytes are provided in Figure 4-3. The XPS spectra of graphite anodes extracted from cells cycled with the MA based electrolytes and STD electrolyte support the generation of a surface film after formation cycling as evidenced by a decrease in the intensity of C-C peak at 285 eV in the C1s spectra, broadening of the O1s spectra characteristic of the O containing species (C=O at 532 eV, C-O at 534 eV) and the appearance of new peaks in the F1s spectra characteristic of LiF at 685 eV and $Li_xPF_yO_z$ at 687 eV. [20,21] The XPS spectra suggest that the anode surface films generated with MA +2% VC and MA+2% FEC are different than the anode surface films derived with cells cycled with STD and MA electrolytes. The surface films derived from MA+2% VC and MA+2% FEC electrolytes contain poly (VC) and poly (FEC) as supported by the presence of a C1s peak at 291 eV and related C=O (532 eV) and C-O (534 eV) peaks in the O1s spectra, which have been previously reported as the decomposition products of VC and FEC.[22,23] In addition, clear differences in F1s spectra are observed with the presence of strong shoulder for $Li_xPF_yO_z$ at 687 eV for the MA+2% VC electrolyte.

The chemical composition of the surface film generated on NCM523 electrode with MA based electrolytes is similar to STD electrolyte (Figure 4-4). Regardless of the electrolyte used in cell cycling, changes in the elemental spectra to the pristine NCM523 remain small. However, a slight change in F1s spectra of the NCM523 electrodes cycled with the STD, MA and MA+2% VC electrolytes is observed as supported by a small shoulder for LiF at 685 eV which is formed from the electrochemical decomposition of $LiPF_6$.[24]

The relative atomic concentration of the initial surface films generated after formation cycling on both graphite and NCM523 electrodes are provided in Table 4-2 and 4-3. There

are no significant changes in elemental concentrations of surface films generated on the NCM523 electrode irrespective of the electrolyte used. However, significant changes are observed on the graphite electrode. The graphite anodes cycled with the STD and MA electrolytes have less carbon and more fluorine compared to the anodes cycled with the MA+2% VC and MA+2% FEC electrolytes. The higher concentrations of fluorine in the former can be attributed to more $LiPF_6$ reduction to generate more LiF while the higher concentrations of oxygen of the anodes cycled with VC or FEC are likely due to the reduction products of the added VC or FEC reduction on graphite.

The IR spectra of graphite and NCM523 surface films after formation cycling are provided in figure 4-5. The IR spectra of graphite surface films generated from all of the different electrolyte formulations have absorptions at 1420 cm^{-1} and 1485 cm^{-1} characteristics of lithium carbonate (Li_2CO_3).[21] In addition, a broad weak absorption characteristic of lithium alkyl carbonates ($ROCO_2Li$) is observed at 1660 cm^{-1} for anodes extracted from cells cycled with the MA electrolyte.[7,20] Incorporation of the electrolyte additives VC or FEC result in the appearance of a broad absorption around 1800 cm^{-1} on graphite formation-cycled with MA+2% VC and MA+2% FEC attributed to the presence of poly (VC) from the reduction of VC or FEC.[22] In addition, the intensity of the absorption of Li_2CO_3 at 1420 cm^{-1} is stronger for the electrolytes containing VC or FEC, consistent with previous reports of Li_2CO_3 generation in the presence of VC or FEC.[25] Alternatively, the IR spectra of the NCM523 electrodes extracted from cells cycled with the different electrolytes are all similar to the pristine NCM523 electrodes. The absence of new absorptions suggests there is no significant accumulation of electrolyte decomposition products on the surface of the cathode. The IR spectra for both the graphite and NCM523 electrodes are consistent with

the XPS data after formation cycling, as discussed above.

Since the XPS spectra and elemental concentrations (Figures 4-6 and 4-7, Table 4-4 and 4-5) and IR spectra (Figure 4-8) of the electrodes (anode and cathode) extracted from the cells cycled with MP based electrolytes are similar to the electrodes extracted from cells cycled with MA based electrolytes, the spectra and tables are included in the supporting information.

Electrolyte formulations containing esters as co-solvents have been reported to have excellent cycling performance at low temperature but upon long-term cycling/accelerated aging conditions cells containing esters have less capacity retention. Therefore, changes in surface chemistry and evolution of the surface films under accelerated aging conditions have been investigated. Cells were cycled at the moderately elevated temperature of 45 ˚C to simulate accelerated aging. Unlike the XPS spectra after formation cycling, the surface of both graphite and NCM523 electrodes change consistent with additional electrolyte decomposition upon accelerated age cycling. The C1s, O1s, F1s and P2p spectra of the graphite anodes cycled in MA based electrolytes after 100 cycles are provided in Figure 4-9. The XPS spectra of the graphite anode cycled with the MA+2 %VC electrolyte evolves significantly relative to the XPS spectra of graphite electrodes cycled with other electrolytes upon cycling at 45 ˚C. This is evident by the increased peak intensities characteristic of poly (VC) at 291 and 287 eV in the C1s spectrum and broadening of related peaks at ~533 eV in the O1s spectrum. The changes observed in peak intensities and peak broadening are consistent with an increase in the concentration of poly (VC) and thickening of the SEI. The larger changes in surface composition are likely due to the presence of plated lithium on the surface of the electrode as observed by SEM and

discussed above. In the presence of STD and MA electrolytes, similar changes in XPS spectra were detected in C1s and related O1s spectra for peaks characteristic of lithium alkyl carbonates and lithium carbonates (290 eV). However, the graphite anode cycled with MA+2% FEC has relatively lower peak intensities for C-O (287 eV), CO_2 (289 eV) and CO_3 (290 eV) in the C1s spectrum suggesting the presence of a thinner surface film after additional cycling.[26] The F1s spectra of graphite anodes cycled with the different electrolytes have two peaks characteristics of LiF at 685 eV and $Li_xPF_yO_z$ at 687 eV in varying intensities. Interestingly, the graphite electrode cycled with MA+2 %VC electrolyte has a higher $Li_xPF_yO_z$ to LiF ratio while the F1s spectra of graphite electrodes cycled with other electrolytes are dominated by the LiF peak. However, an increase in the peak intensity of $Li_xPF_yO_z$ (687 eV) is observed upon extended cycling for the MA, STD, and MA+2% FEC electrolytes suggesting additional generation of lithium fluorophosphate spices from the decomposition of $LiPF_6$. The significant increase in lithium fluorophosphate species upon extended cycling at 45 ˚C is further supported by the presence of a strong peak at 134 eV in the P2p spectra.

The relative atomic concentration of the surface films generated on graphite electrode after 100 cycles is provided in table 4-6. Significant changes in relative atomic concentrations are observed for all the electrolytes, with a decrease in carbon and fluorine and an increase in oxygen and phosphorus. The changes in elemental concentrations are consistent with the anode elemental XPS spectra upon extended cycling and suggest thickening of the SEI by further electrolyte decomposition upon extended cycling.

The C1s, F1s, O1s and P2p XPS spectra of the NCM 523 cathodes after 100 cycles are presented in Figure 4-10. Upon extended cycling, the deposition of a relatively thin cathode

surface film is observed with all of the electrolytes, evidenced by reduced intensity of the metal oxide peak at 530 eV in O1s spectra.[27] However, generation of more O-species is apparent for cells cycled with MA+2% FEC, where the intensity of the C-C peak at 285 eV is reduced and the intensities of the C-O at 287 eV and CO_2 at 289 eV peaks are increased in C1s spectrum. In addition, cathodes cycled with the STD, MA and MA+2% VC electrolytes have a significant shoulder for LiF (685 eV) in F1s spectra with relatively similar peak intensities and relative atomic percentage to the electrodes analyzed after formation cycling (figure 4-4 and table 4-3). Moreover, there are only weak peaks in P2p spectra on the cathode compared to that of the anode, suggesting that no further reaction of $LiPF_6$ has occurred on the cathode during extended cycling. However, detection of less carbon and more oxygen (Table 4-7) upon extended cycling in the cathode surface film for all the electrolyte formulations suggests that further oxidation of solvents may occur to generate on organic rich CEI.[28] As observed for electrodes analyzed after formation cycling, the XPS spectra of graphite (Figure 4-11) and NCM523 (Figure 4-12) electrodes after extended cycling in MP based electrolytes have similar chemical composition and elemental concentrations (Table 4-8 and 4-9) to corresponding MA based electrolytes.

The IR-ATR spectra of graphite anodes and NCM523 cathodes containing MA based electrolytes after 100 cycles are presented in Figure 4-13. The IR spectra of graphite electrodes cycled with MA based electrolytes are similar to the electrodes cycled with the STD electrolyte and are dominated by strong absorptions characteristic of lithium carbonate (Li_2CO_3) at 1420 cm^{-1} and 1480 cm^{-1} and lithium alkyl carbonate (ROCOOLi) at 1608 cm^{-1}. In addition, the electrodes cycled with the MA+2% FEC electrolyte contain an additional IR absorption at 1800 cm^{-1} attributed to polycarbonate resulting from the

reduction of FEC to generate poly (VC).[22] The increased intensities for these absorptions are consistent with the XPS data and evolution of the SEI upon extended cycling. It should be noted that the IR spectrum for the electrode cycled with the MA+2% VC electrolyte was not acquired due evidence of lithium plating on the surface and the high reactivity of lithium metal with the germanium crystal of the ATR accessory. IR-ATR spectra of the cathodes cycled with MA+2% FEC electrolyte contain strong absorption peaks characteristic of Li_2CO_3 at 1430 cm^{-1} and 1485 cm^{-1}, and lithium alkyl carbonate at 1608 cm^{-1}. The IR spectra of the cathodes cycled with either the STD electrolyte or the MA electrolyte are dominated by peaks characteristic of the PVDF binder.[29]

CONCLUSIONS

This investigation has focused on the *ex-situ* surface analysis of electrodes extracted from NCM523/graphite cells containing methyl acetate (MA) and methyl propionate (MP) esters as co-solvents in electrolyte formulations. These electrolyte formulations have been previously reported as some of the most promising formulations designed for improved low temperature performance without compromising calendar life. The cycling performance was investigated over a wide operating temperature range (-20 ˚C to 45 ˚C) to better understand the stability of the SEI generated from the ester-based formulations for moderately elevated temperature applications, such as electric vehicles. Some formulations included FEC or VC as electrolyte additives to improve the performance at moderately elevated temperature. While both MA and MP based ester formulations improve the low temperature discharge capacities compared to cells containing the STD electrolyte, the cells containing the ester formulations have more capacity fade upon cycling at 45 º. Addition of FEC as an electrolyte additive improves the low temperature cycling performance and improves the elevated temperature cycling stability for the MA based ester formulation, suggesting the lithium-ion intercalation /de-intercalation kinetics are more favorable with cells containing MA as a co-solvent and FEC as an electrolyte additive. The improved performance at elevated temperature is likely due to changes in the composition of the anode SEI which result in the generation of a more stable anode SEI. Unfortunately, addition of VC decreases the ambient and high temperature cycling performance after cycling at low temperature with both ester-based electrolyte systems. This is most likely due to lithium plating during low temperature charging which leads to continued electrolyte degradation upon cycling resulting in the generation of a thicker SEI. *Ex-situ* surface analysis of electrodes via a combination of XPS and IR shows significant

changes to the SEI on graphite upon extended cycling with the ester-based electrolytes containing electrolyte additives, especially in the presence of VC. Furthermore, the incorporation of electrolyte additives alters the structure of the surface films on the NCM523 cathodes, especially with FEC.

ACKNOWLEDGMENTS

This work was supported by the Assistant Secretary for Energy Efficiency and Renewable Energy, Vehicle Technology Office of the U.S. DOE through Applied Battery Research for Transportation (ABRT) program under contract No. DE-SC0012704.

REFERENCES

1. S. S. Zhang, K. Xu, and T. R. Jow, *Journal of Power Sources*, **115**, 137–140 (2003).

2. K. Xu, *Chemical Reviews*, **104**, 4303–4417 (2004).

3. T. R. Jow, M. S. Ding, K. Xu, S. S. Zhang, J. L. Allen, K. Amine, and G. L. Henriksen, *Journal of Power Sources*, **119**–**121**, 343–348 (2003).

4. S. S. Zhang, K. Xu, and T. R. Jow, *Electrochimica Acta*, **48**, 241–246 (2002).

5. N. D. Rodrigo, S. Tan, Z. Shadike, E. Hu, X.-Q. Yang, and B. L. Lucht, *Journal of The Electrochemical Society*, **168**, 070527 (2021).

6. Q. Li, S. Jiao, L. Luo, M. S. Ding, J. Zheng, S. S. Cartmell, C.-M. Wang, K. Xu, J.-G. Zhang, and W. Xu, *ACS Applied Materials and Interfaces*, **9**, 18826–18835 (2017).

7. M. C. Smart, B. L. Lucht, S. Dalavi, F. C. Krause, and B. V. Ratnakumar, *Journal of The Electrochemical Society*, **159**, A739–A751 (2012).

8. S. S. Zhang, K. Xu, and T. R. Jow, *Electrochemistry Communications*, **4**, 928–932 (2002).

9. M. C. Smart, B. V. Ratnakumar, V. S. Rayan-Mowrey, S. Surampudi, G. K. S. Prakash, J. Hu, and I. Cheung, *Journal of Power Sources*, **119**–**121**, 359–367 (2003).

10. J. Kim, V. A. K. Adiraju, O. B. Chae, and B. L. Lucht, *Journal of The Electrochemical Society*, **168**, 080538 (2021).

11. B. Yang, H. Zhang, L. Yu, W. Z. Fan, and D. Huang, *Electrochimica Acta*, **221**, 107–114 (2016).

12. E. R. Logan, E. M. Tonia, K. L. Gering, J. Li, X. Ma, L. Y. Beaulieu, and J. R. Dahn, *Journal of The Electrochemical Society*, **165**, A21–A30 (2018).

13. M. C. Smart, B. V. Ratnakumar, K. B. Chin, and L. D. Whitcanack, *Journal of The Electrochemical Society*, **157**, A1361 (2010).

14. X. Ma, R. S. Arumugam, L. Ma, E. Logan, E. Tonita, J. Xia, R. Petibon, S. Kohn, and J. R. Dahn, *Journal of The Electrochemical Society*, **164**, A3556–A3562 (2017).

15. X. Ma, J. Li, S. L. Glazier, L. Ma, K. L. Gering, and J. R. Dahn, *Electrochimica Acta*, **270**, 215–223 (2018).

16. M. C. Smart, B. V. Ratnakumar, and S. Surampudi, *Journal of The Electrochemical Society*, **149**, A361 (2002).

17. J.-P. Jones, M. C. Smart, F. C. Krause, and R. V. Bugga, *Journal of The Electrochemical Society*, **167**, 020536 (2020).

18. J. Wandt, P. Jakes, J. Granwehr, R. A. Eichel, and H. A. Gasteiger, *Materials Today*, **21**, 231–240 (2018).

19. T. Foroozan, S. Sharifi-Asl, and R. Shahbazian-Yassar, *Journal of Power Sources*, **461**, 228135 (2020).

20. M. Nie, D. Chalasani, D. P. Abraham, Y. Chen, A. Bose, and B. L. Lucht, *Journal of Physical Chemistry C*, **117**, 1257–1267 (2013).

21. P. Verma, P. Maire, and P. Novák, *Electrochimica Acta*, **55**, 6332–6341 (2010).

22. A. L. Michan, B. S. Parimalam, M. Leskes, R. N. Kerber, T. Yoon, C. P. Grey, and B. L. Lucht, *Chemistry of Materials*, **28**, 8149–8159 (2016).

23. E. Markevich, G. Salitra, and D. Aurbach, *ACS Energy Letters*, **2**, 1337–1345 (2017).

24. S. K. Heiskanen, J. Kim, and B. L. Lucht, *Joule*, **3**, 2322–2333 (2019).

25. K. U. Schwenke, S. Solchenbach, J. Demeaux, B. L. Lucht, and H. A. Gasteiger, *Journal of The Electrochemical Society*, **166**, A2035–A2047 (2019).

26. H. B. Son, M.-Y. Jeong, J.-G. Han, K. Kim, K. H. Kim, K.-M. Jeong, and N.-S. Choi, *Journal of Power Sources*, **400**, 147–156 (2018).

27. W. Li, and B. L. Lucht, *Journal of Power Sources*, **168**, 258–264 (2007).

28. J. A. Gilbert, J. Bareńo, T. Spila, S. E. Trask, D. J. Miller, B. J. Polzin, A. N. Jansen, and D. P. Abraham, *Journal of The Electrochemical Society*, **164**, A6054–A6065 (2017).

29. T. Liu, A. Garsuch, F. Chesneau, and B. L. Lucht, *Journal of Power Sources*, **269**, 920–926 (2014).

FIGURES

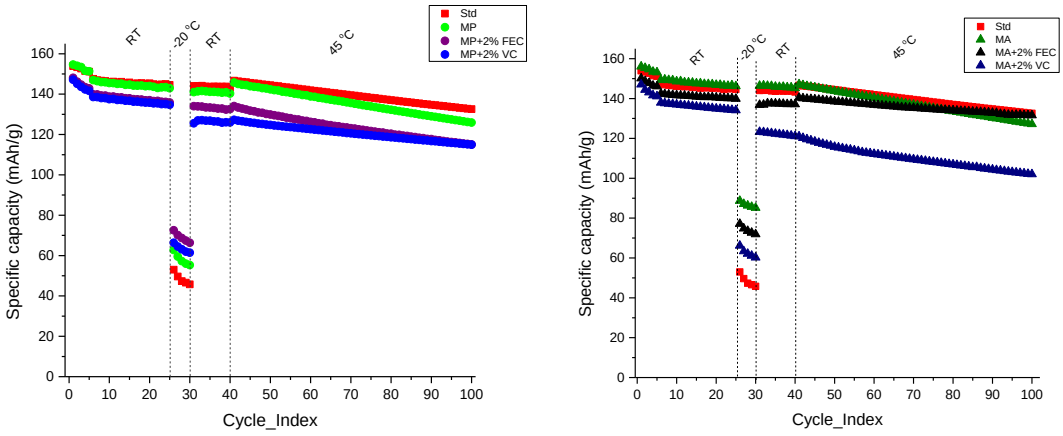

Figure 4-1. Specific capacities of graphite/NCM523 full cells with MP (left) and MA (right) based electrolytes over wide operating temperature range.

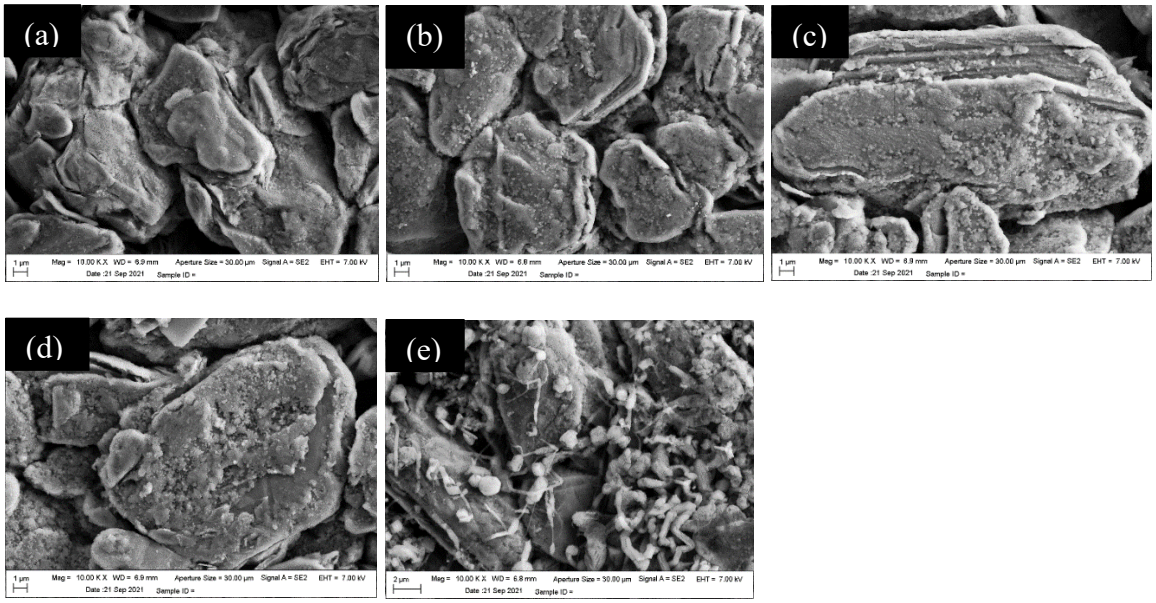

Figure 4-2. FE-SEM images of (a) Pristine graphite and cycled graphite electrodes in (b) STD (c) MA (d) MA+2% FEC and (e) MA+2% VC electrolytes after 100 cycles.

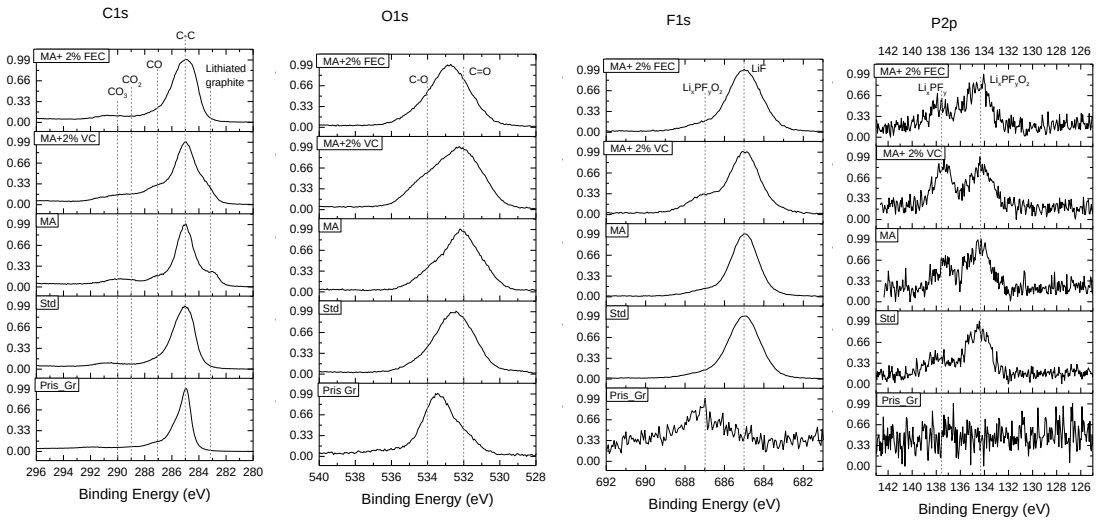

Figure 4-3. C1s, O1s, F1s and P2p XPS spectra of graphite anodes for MA based electrolytes after formation cycling.

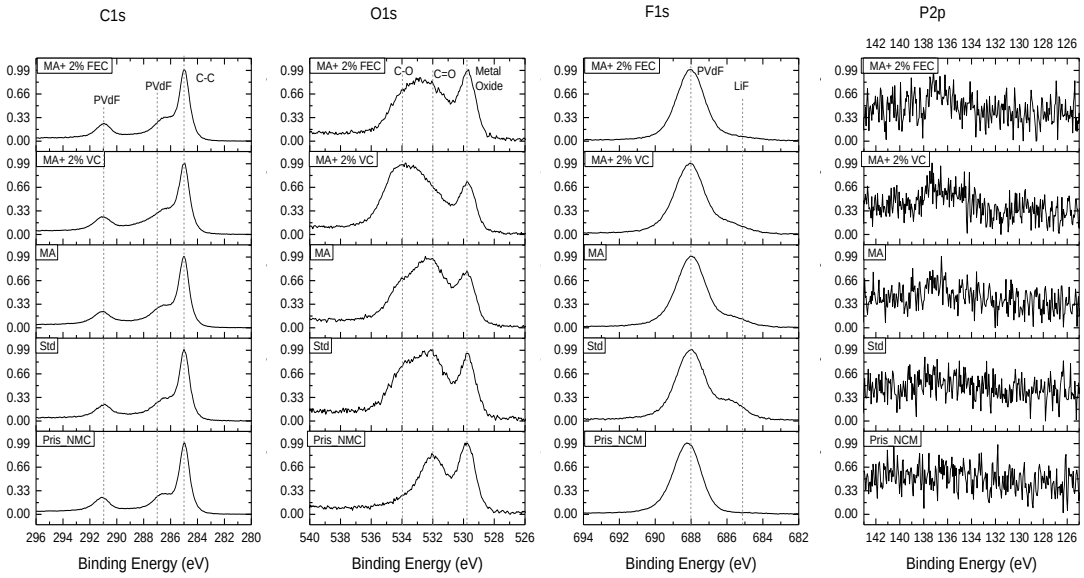

Figure 4-4. C1s, O1s, F1s and P2p XPS spectra of NCM523 cathodes for MA based electrolytes after formation cycling.

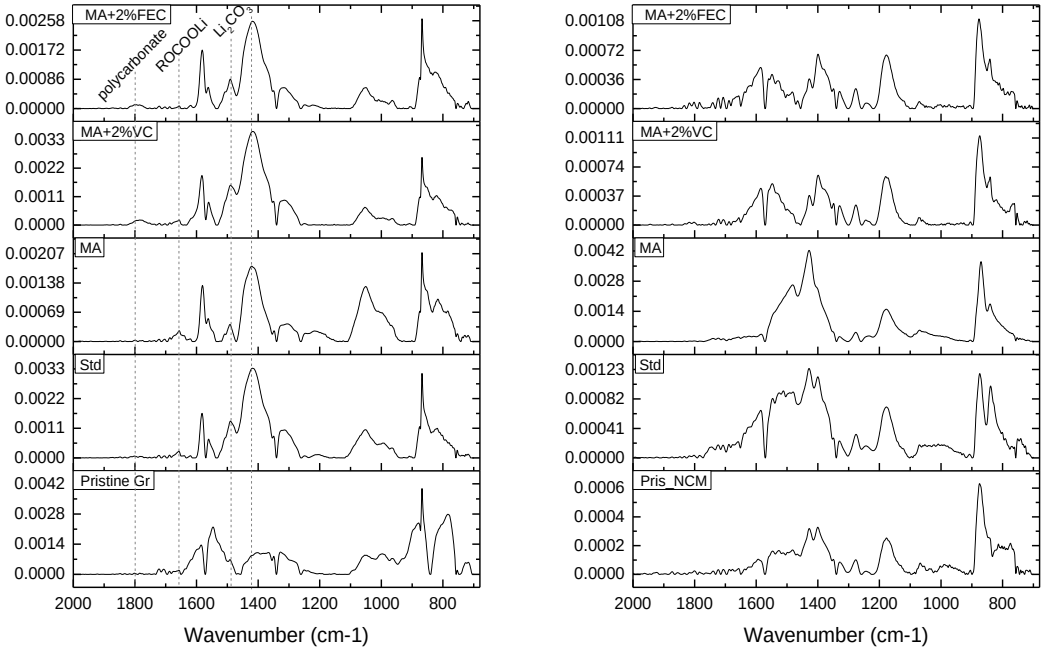

Figure 4-5. IR spectra of MA based graphite anodes (left) and MA based NCM523 cathodes (right) after formation cycling.

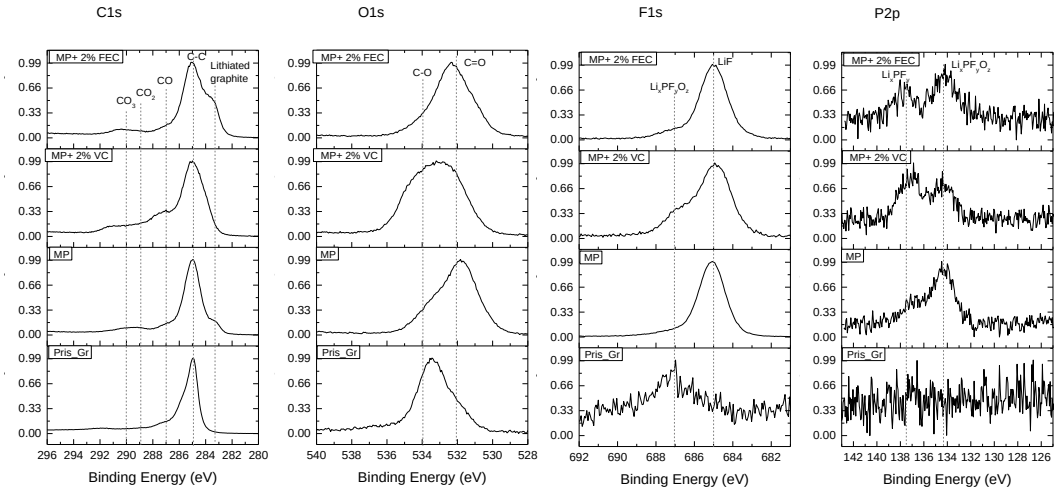

Figure 4-6. C1s, O1s, F1s and P2p XPS spectra of graphite anodes for MP based electrolytes after formation cycling.

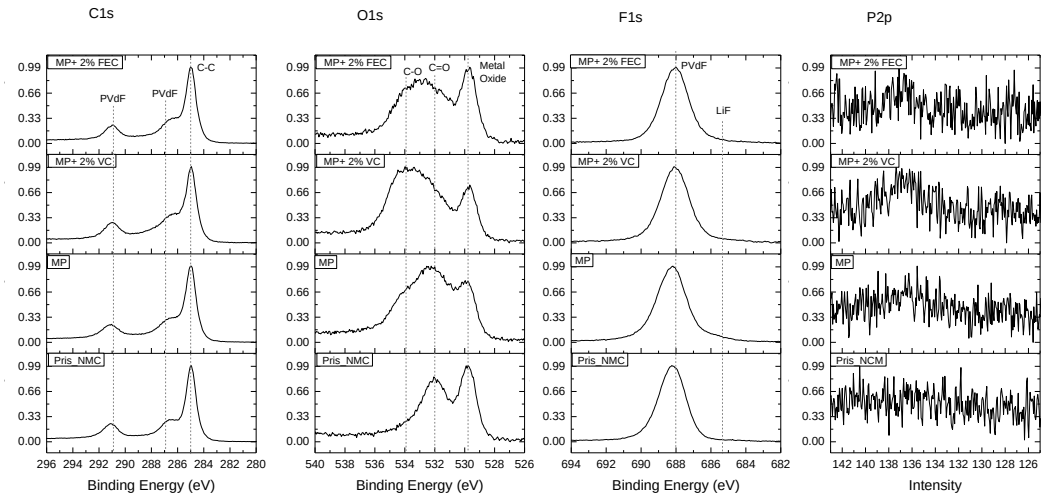

Figure 4-7. C1s, O1s, F1s and P2p XPS spectra of NCM523 cathodes for MP based electrolytes after formation cycling

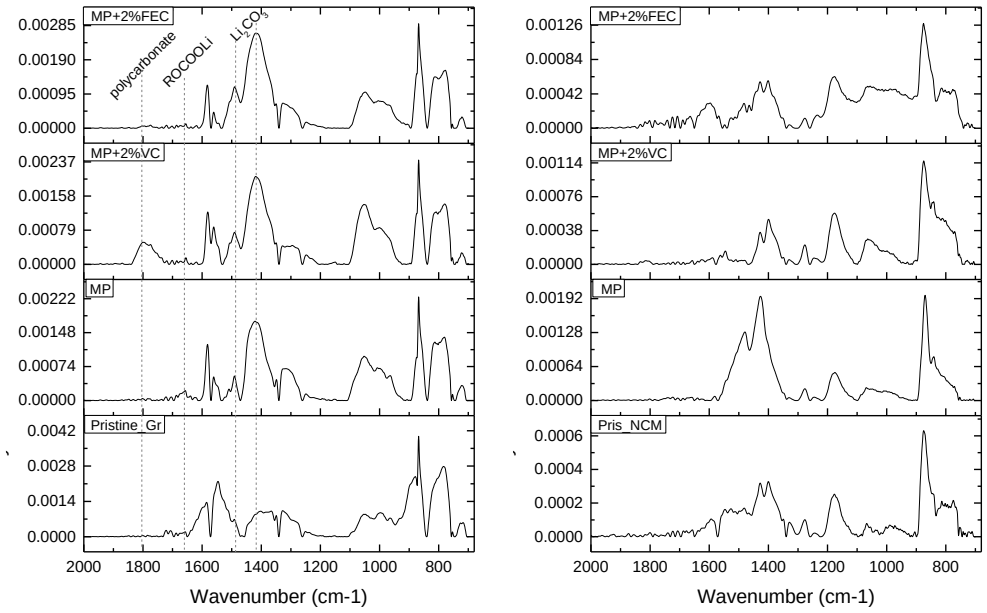

Figure 4-8. IR spectra of MP based graphite anodes (left) and MP based NCM523 cathodes (right) after formation cycling

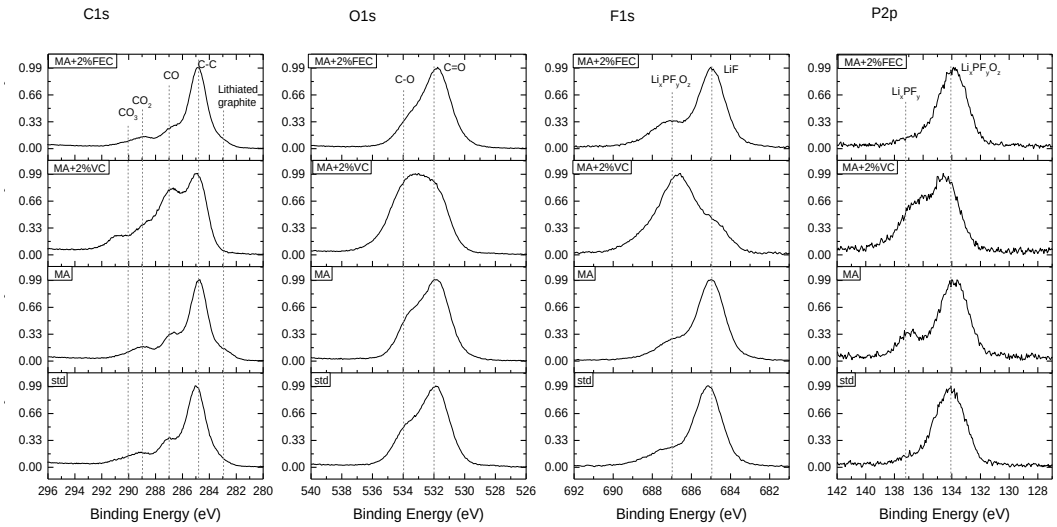

Figure 4-9. C1s, O1s, F1s and P2p XPS spectra of graphite anodes for MA based electrolytes after 100 cycles.

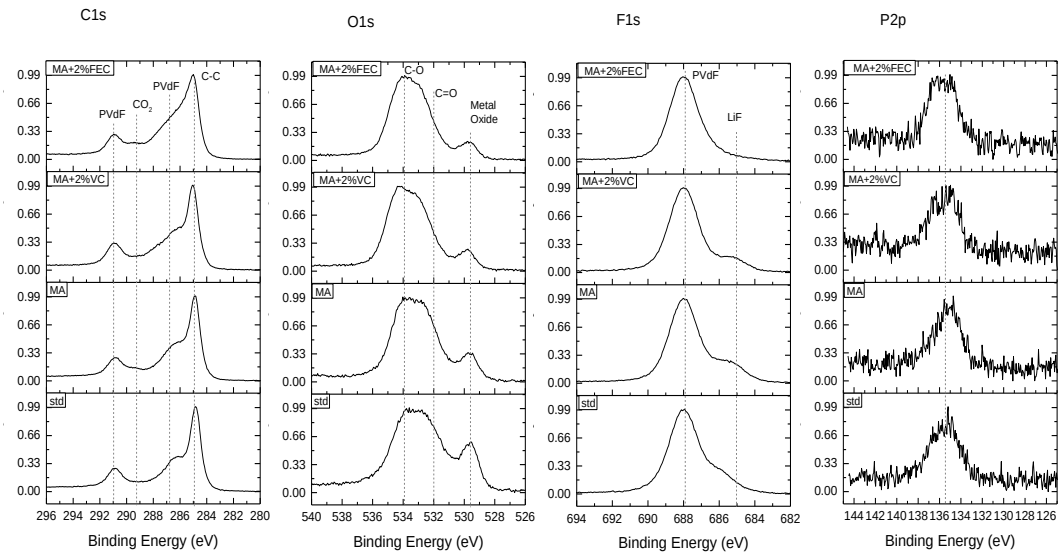

Figure 4-10. C1s, O1s, F1s and P2p XPS spectra of NCM523 cathodes for MA based electrolytes after 100 cycles.

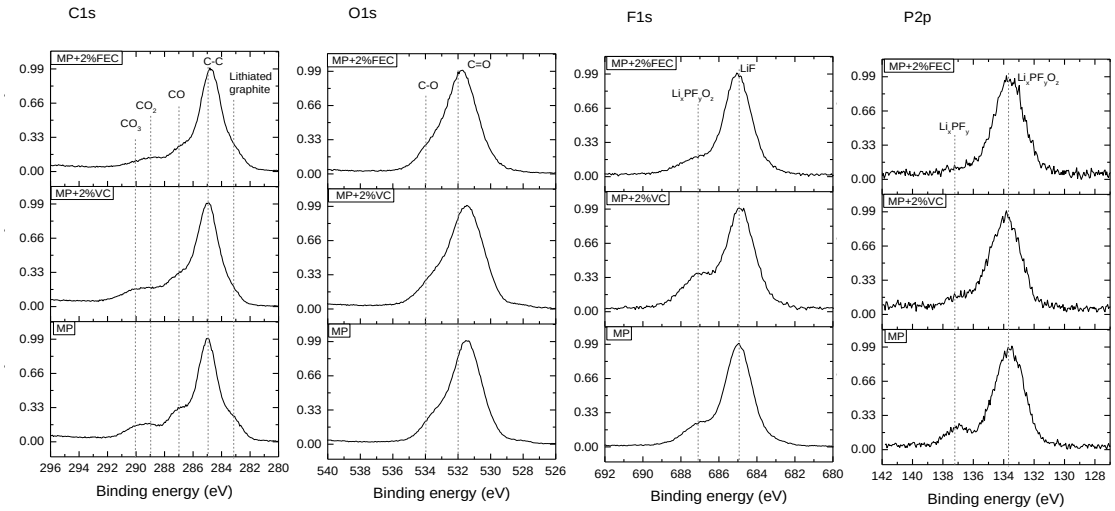

Figure 4-11. C1s, O1s, F1s and P2p XPS spectra of graphite anodes for MP based electrolytes after 100 cycles

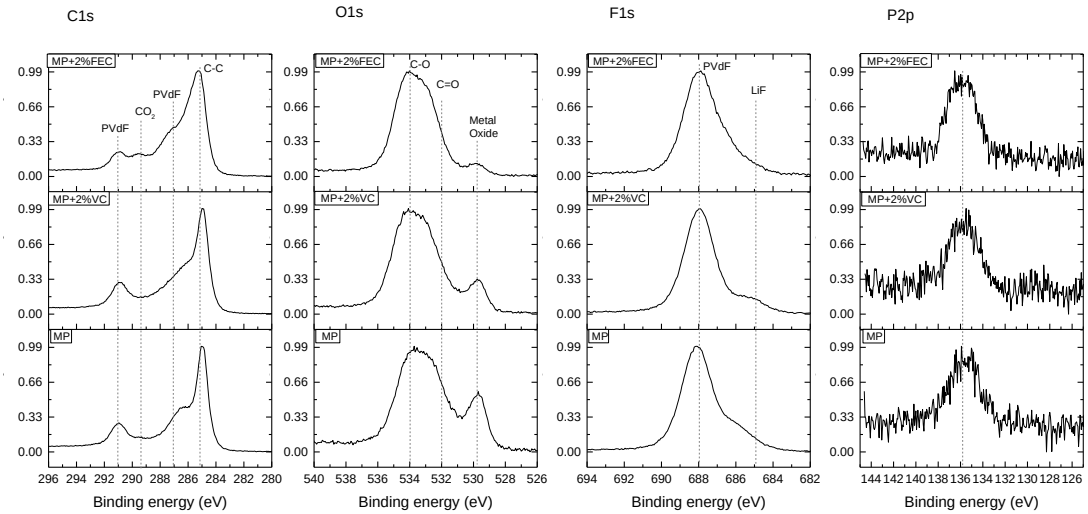

Figure 4-12. C1s, O1s, F1s and P2p XPS spectra of NCM523 cathodes for MP based electrolytes after 100 cycles.

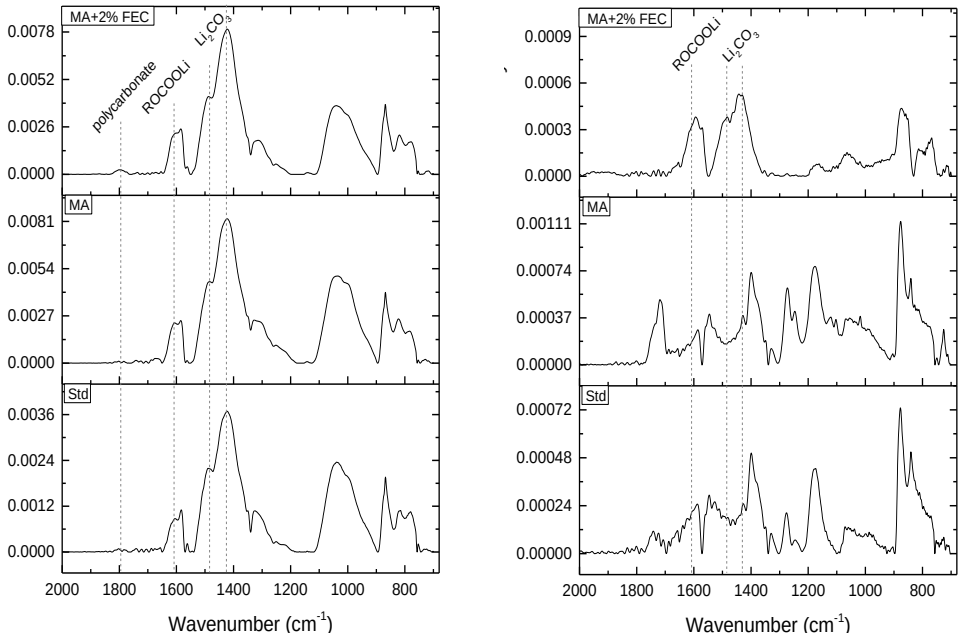

Figure 4-13. IR spectra of MA based graphite anodes (left) and MA based NCM523 cathodes (right) after 100 cycles.

TABLES

Table 4-1. Electrolyte formulations

Electrolyte	Electrolyte formulation
STD	1.2 M $LiPF_6$ in EC: EMC (3:7 vol %)
MA	1.2 M $LiPF_6$ in EC: EMC: MA (20: 60: 20 vol %)
MP	1.2 M $LiPF_6$ in EC: EMC: MP (20: 60: 20 vol %)
MA + 2% VC	1.2 M $LiPF_6$ in EC: EMC: MA (20: 60: 20 vol %) + 2% VC (vol %)
MP + 2% VC	1.2 M $LiPF_6$ in EC: EMC: MP (20: 60: 20 vol %) + 2% VC (vol %)
MA + 2% FEC	1.2 M $LiPF_6$ in EC: EMC: MA (20: 60: 20 vol %) + 2% FEC (vol %)
MP + 2% FEC	1.2 M $LiPF_6$ in EC: EMC: MP (20: 60: 20 vol %) + 2% FEC (vol %)

Table 4-2. Corresponding relative atomic concentrations from XPS elemental spectra obtained for graphite anode after formation cycling in MA based electrolytes

	C	O	F
Pristine Graphite	91.5	8.6	
STD	56.3	19.6	24.1
MA	52.0	20.5	27.5
MA+2% VC	60.8	28.5	10.7
MA+2% FEC	63.4	20.1	16.5

Table 4-3. Corresponding relative atomic concentrations from XPS elemental spectra obtained for NCM523 cathodes after formation cycling in MA based electrolytes.

	C	O	F
Pristine NCM523	69.6	6.9	23.5
STD	66.1	10.9	23.0
MA	67.1	10.3	22.6
MA+2% VC	65.1	13.7	21.2
MA+2% FEC	68.1	9.3	22.6

Table 4-4. Corresponding Relative atomic concentrations from XPS elemental spectra obtained for graphite anode after formation cycling in MP based electrolytes.

	C	O	F
MP	55.9	18.8	25.4
MP+2% VC	63.1	27.5	9.4
MP+2% FEC	67.2	19.5	13.4

Table 4-5. Corresponding Relative atomic concentrations from XPS elemental spectra obtained for NCM523 cathodes after formation cycling in MP based electrolytes.

	C	O	F
MP	67.5	11.0	21.6
MP+2% VC	65.0	13.8	21.2
MP+2% FEC	69.0	9.5	21.5

Table 4-6. Corresponding relative atomic concentrations from XPS elemental spectra obtained for graphite anode after 100 cycles in MA based electrolytes.

	C	O	F	P
Pristine Graphite	91.5	8.6		
STD	48.8	31.7	15.5	4.0
MA	46.7	27.3	22.7	3.4
MA+2% VC	50.9	34.9	11.0	3.2
MA+2% FEC	55.5	30.5	10.1	3.9

Table 4-7. Corresponding relative atomic concentrations from XPS elemental spectra obtained for NCM523 cathodes after 100 cycles in MA based electrolytes.

	C	O	F
Pristine NCM523	69.6	6.9	23.5
STD	62.3	13.3	24.5
MA	63.9	13.4	22.7
MA+2% VC	62.0	17.0	20.9
MA+2% FEC	65.4	18.7	15.9

Table 4-8. Corresponding Relative atomic concentrations from XPS elemental spectra obtained for graphite anode after 100 cycles in MP based electrolytes.

	C	O	F	P
MP	41.8	30.5	23.6	4.1
MP+2% VC	54.5	34.7	8.0	2.8
MP+2% FEC	53.0	31.2	12.0	3.9

Table 4-9. Corresponding Relative atomic concentrations from XPS elemental spectra obtained for NCM523 cathodes after 100 cycles in MP based electrolytes.

	C	O	F
MP	63.0	13.4	23.6
MP+2% VC	63.5	17.0	19.5
MP+2% FEC	67.4	20.9	11.7